Interval spectral stochastic finite element analysis of structures with aggregation of random field and bounded parameters

Duy Minh Do[1], Wei Gao[1], Chongmin Song[1] and Michael Beer[2]

[1] Centre for Infrastructure Engineering and Safety (CIES), School of Civil and Environmental Engineering, The University of New South Wales, Sydney, NSW 2052, Australia

Email addresses: duy.m.do@unsw.edu.au, duy.m.do@gmail.com (D.M. Do); w.gao@unsw.edu.au (W. Gao).

[2] Institute for Computer Science in Civil Engineering, Leibniz University Hannover 30167 Hannover, Germany

SUMMARY

This paper presents the study on non-deterministic problems of structures with a mixture of random field and interval material properties under uncertain-but-bounded forces. Probabilistic framework is extended to handle the mixed uncertainties from structural parameters and loads by incorporating interval algorithms into spectral stochastic finite element method. Random interval formulations are developed based on K-L expansion and polynomial chaos accommodating the random field Young's modulus, interval Poisson's ratios and bounded applied forces. Numerical characteristics including mean value and standard deviation of the interval random structural responses are consequently obtained as intervals rather than deterministic values. The randomised low-discrepancy sequences initialized particles and high-order nonlinear inertia weight with multi-dimensional parameters is employed to determine the change ranges of statistical moments of the random interval structural responses. The bounded probability density and cumulative distribution of the interval random response are then visualised. The feasibility, efficiency and usefulness of the proposed interval spectral stochastic finite element method are illustrated by three numerical examples.

Keywords: interval spectral stochastic finite element method; random field; hybrid uncertainty; interval random response; bounding probabilistic distribution functions.

1. INTRODUCTION

The considerable influences of inevitable uncertainties in engineering problems have stimulated more and more studies on stochastic analysis to investigate possible predictions of engineering systems responses [1-5]. The framework of stochastic assessment implemented

by deterministic operators considering random inputs has been well-developed with applications in engineering mechanics and other research areas. The analysis becomes much more complicated when random operators are adopted to handle uncertainties as their performance relates to the degree of complexity of mathematical tools for modelling engineering systems. Moreover, the degree of complexity is considerably augmented for large scale engineering problems with intrinsic interaction among different elements of systems as well as with the interaction of the systems and their surrounding environments. These issues create major challenges for our numerical algorithms to be reliable, close to reality and efficient when mathematical and mechanical models are established for real engineering systems [6]. A current powerful tool in computational stochastic mechanics satisfying the requirements to a large extent is the spectral stochastic finite element method (SSFEM) introduced by Ghanem and Spanos [7]. The SSFEM is a seminal improvement of the standard deterministic finite element method with its feature to capture random physics in a comprehensive and natural manner in a stochastic framework efficiently. Its efficiency is proved by many studies and has been constantly improved to attain more accurate results [8-18]. Compared with other probabilistic methods based on finite element analysis such as sampling and perturbation methods [6, 19, 20], the SSFEM solves stochastic problems in structural engineering in an integrated manner. Further developments in this direction are pursued extensively [18].

A challenging aspect of this general approach for analysing stochastic engineering structures is the modelling of the uncertain structural parameters comprising material property, geometry and loading regime. The awareness of this aspect has emerged from the discussion that structural responses are sensitive to uncertainties in structural parameters and in applied forces. This issue requires putting particular attention to the modelling of the input uncertainty in the SSFEM using random fields of structural parameters. Commonly, uncertain material properties are described with random fields in the SSFEM. The challenge of a large number of random structural parameters and multiple random material properties has been addressed, and extensions to capture random geometric properties as well have been presented [21-24]. On this basis, a large variety of random parameters can be captured in the SSFEM with a mathematical modelling suitable for solving large industrial problems.

This modelling, however, requires substantial information about the uncertainties. In practical cases, in particular in civil engineering, available information about parameters and their uncertainties is often limited [25]. Those cases have motivated an exploration of further uncertainty models, such as intervals and imprecise probabilities, for engineering analyses [26]. These models are compatible with the stochastic framework, specifically in view of the subsequent development, with the SSFEM.

In order to choose an appropriate uncertainty model, the analyst is required to explore the sources of the uncertainty, the information content of the uncertain information and also the

suitability of the models for the purpose of the analysis. A detailed discussion on these issues is provided in [26]. Once the uncertainty model is selected, an efficient numerical algorithm is required for processing to calculate the uncertainty of the structural or system response and related quantities such as the failure probability. Both modelling and numerical processing are well-addressed in the stochastic framework [27, 28]. Probabilistic modelling captures both frequentist quantification based on data and subjectivist quantification with subjective probabilities in form of a belief. As a powerful combination of both, Bayesian approaches have attracted extensive attention and have been developed to a sophisticated level with applicability to large-scale problems [29-33]. The entire framework of stochastic techniques is readily available for the processing of uncertainty modelled in this manner.

On the side of non-probabilistic models developments have been considerably achieved and are applicable in a sophisticated stage for modelling. Key attention is paid to the development of numerically efficient algorithms to enable the analysis of large frequentist problems [34, 35]. In the present paper we contribute to the development of numerically efficient algorithms in the case of combined random and interval-valued structural parameters.

We address the class of problems, where only lower and upper bounds are known for some structural parameters [36] rather than a statistical data base or a subjective belief in form of a distribution function. For a detailed reasoning in this regard, see [26]. In those cases, interval modelling, firstly developed by Moore [37], is typically proposed to represent the uncertain variables . Interval approaches alone, however, have only limited applicability because most of the practical cases involve uncertainty with both random nature and interval nature. Hence, hybrid models, such as interval probabilities, and associated techniques have been developed and applied in structural engineering [38-46]. In this manner, random and interval variables are considered simultaneously and maintain their characteristics throughout the entire analysis. This concept is adopted herein to combine the powerful model of random fields with interval variables for those parameters for which only bounded information is available. The focus of the development is on the numerical side, providing an efficient algorithm for the processing of the mixed interval probabilistic uncertainty.

Specifically, in this paper, random fields are combined with interval analysis addressing bounded uncertainty parameters in the context of the SSFEM. This combination poses challenges as the mixed stochastic interval problems needs to be solved at mathematical level and at physically practical level for real engineering applications [47]. Random structural responses in the SSFEM can be characterised by statistical moments, e.g. the first two moments, mean value and standard deviation. Interval analysis can provide interval values for the responses. A combination of the SSFEM and interval analysis as interval spectral stochastic finite element method (ISSFEM) is, consequently, able to produce intervals that represent the moments of interval random responses. That is, an interval mean and an interval standard deviation will be obtained. More generally, an entire set of probabilistic responses is

obtained instead of a single probabilistic response, whereby intervals work as set-theoretical descriptors in probabilistic models. The cardinality of this set of probabilistic responses, or simply the size of the intervals for the moments, reflects the entire combined bounded uncertainty in form of intervals from the input. The assessment of the output of ISSFEM can still utilize the complete probabilistic information, but now with the additional feature of knowing bounds on these probabilities. Also, the numerical processing of the probabilistic information can still be performed with powerful stochastic technologies, such as Monte Carlo simulation, and be combined with interval analysis to process the intervals. However, Monte Carlo simulation requires a considerable numerical effort, which can easily make an interval probabilistic analysis infeasible when a repeated simulation is necessary as it is the case in non-intrusive approaches such as global optimization [48]. This problem is specifically critical in the case of large structures with a large number of interval parameters − unless specific topological properties can be exploited in the search domain [49]. On the other hand, intrusive methods, implementing interval arithmetic directly into the numerical algorithms, are always limited to small problem classes and require a tremendous effort of implementation [50, 51]. Moreover, the ordinary algebra suffers from the so-called dependency. To limit the catastrophic effects of the dependency phenomenon, Muscolino and Sofi [42] presented an improvement of the interval arithmetic by introducing a particular unitary interval and the presented procedure has substantially improved the accuracy as interval amplitude of the uncertain parameters increases. Recently, a new uncertain analysis method based on Chebyshev inclusion functions is proposed to effectively achieve bounds for meaningful solutions of interval functions for multibody dynamics of mechanical systems and vehicle dynamics [46, 52] even sometimes the numerical simulation may still experience small overestimation. It is worth mentioning that scanning methods [53] and combinatorial approach [54] may be able to produce accurate bounds, but they are only applicable for the problems with small number of interval variables. Non-intrusive methods such as global optimization are much more general and easier to establish. Furthermore, it can commendably control overestimation of the interval computation and the dependency phenomenon does not exist when it is adopted to solve interval analysis. Thus, we implement interval analysis to find the set of probabilistic system outputs in terms of bounds on probabilistic parameters and probabilities in the form of a global optimization. In order to cope with the numerical cost of the optimization involved, we propose an efficient optimization strategy that does not compromise the accuracy of the results. Among the algorithms available to solve the involved optimization, the particle swarm optimization (PSO) proposed by Kennedy and Eberhart [55] shows particularly attractive efficiency features [56, 57]. This method requires only a small number of iterations to attain high-quality results. We adopt the basic concept of this algorithm and propose an improvement based on randomised low-discrepancy sequences initialized particles and high-order nonlinear inertia weight, denoted as RLHNPSO. This algorithm is employed with multi-dimensional parameters to investigate the interval random structural response through the

combination with the SSFEM, denoted as ISSFEM. The results are obtained as sets of probability distributions described by interval parameters and intervals for probabilities.

The paper is organized as follows. In Section 2, the concept of ISSFEM is built up by introducing interval uncertainty into the spectral stochastic finite element method. Section 3 presents the incorporation of the randomised low-discrepancy sequences initialized high-order nonlinear particle swarm optimization algorithm into ISSFEM with respect to investigation of the possible ranges of statistical moments for the interval random outputs. Section 4 illustrates the performance of the proposed ISSFEM by three numerical examples. Finally, a discussion and concluding remarks are provided in Section 5.

2. CONCEPT OF INTERVAL SPECTRAL STOCHASTIC FINITE ELEMENT METHOD

In real engineering applications, the uncertainty models of different parameters can be different when the mathematical presentation for each uncertainty parameter is modelled by using the available sufficient and/or insufficient data. The challenge problem posed here is to aggregate the disparate representation of different types of uncertain parameters into a single uncertainty model of system, leading to a hybrid mathematical form. This section presents the general mathematical expressions for the interval spectral stochastic finite element method developed from the framework of spectral stochastic finite element analysis. The random field simulation is combined with interval arithmetic to describe the uncertainty parameters. This work is motivated by the awareness of the uncertainty modelling for different parameters in the SSFEM [21-24] as well as by the considerations of the mixture of mathematical models for addressing different types of uncertainty parameters including random and interval variables [39-41, 43].

For a general deterministic two-dimensional problem, the constitutive matrix D is given by:

$$D = E \cdot Q(v) \tag{1}$$

where matrix $Q(v)$ is the function of Poisson's ratio v.

For material property characterized as uncertainty feature, constitutive matrix is examined into the case of incorporation among different models of uncertainty. In this study, it not only considers the spatial variation of the elastic modulus, but also the uncertainty of Poisson's ratio. These uncertainty variables are assumed to be independent to each other [23]. The uncertainty of the elastic modulus is described by a random field while the uncertainty of the Poisson's ratio is assumed to be represented by intervals. For plane stress problems, the interval random constitutive matrix can be expressed as:

$$D^I(x,\theta) = D\big(E(x,\theta),v^I\big) = E(x,\theta)\cdot Q(v^I)$$

$$= E_0 R(x,\theta)\left(\frac{1}{1-\left(v^I\right)^2}\right)\begin{bmatrix} 1 & v^I & 0 \\ v^I & 1 & 0 \\ 0 & 0 & \dfrac{1-v^I}{2} \end{bmatrix} \tag{2}$$

For plane strain problems, we have:

$$D^I(x,\theta) = D\big(E(x,\theta),v^I\big) = E(x,\theta)\cdot Q(v^I)$$

$$= E_0 R(x,\theta)\left(\frac{1}{\left(1+v^I\right)\left(1-2v^I\right)}\right)\begin{bmatrix} 1-v^I & v^I & 0 \\ v^I & 1-v^I & 0 \\ 0 & 0 & \dfrac{1-2v^I}{2} \end{bmatrix} \tag{3}$$

where E_0 is the mean value of elastic modulus; v^I is the interval Poisson's ratio and its change range is denoted as $[\underline{v},\overline{v}]$ with lower bound value $\underline{v}$ and upper bound value $\overline{v}$. v^I can be dissimilar from each other for different elements. $R(x,\theta)$ is a homogeneous Gaussian field of unit mean and can be represented by using K-L expansion:

$$R(x,\theta) = 1 + \sum_{i=1}^{\infty}\omega_i(x)\xi_i(\theta) = 1 + \sum_{i=1}^{\infty}\sqrt{\lambda_i}\phi_i(x)\xi_i(\theta) \tag{4}$$

Then, the random field of elastic modulus can be expressed as:

$$E(x,\theta) = E_0\left(1 + \sum_{i=1}^{\infty}\sqrt{\lambda_i}\phi_i(x)\xi_i(\theta)\right) = E_0\left(1 + \sum_{i=1}^{\infty}\omega_i(x)\xi_i(\theta)\right) \tag{5}$$

where $\xi_i(\theta)(i=1,2,\ldots)$ are mutually uncorrelated random variables, λ_i and $\phi_i(x)$ are correspondingly the eigenvalues and eigenfunctions of $C(x_1,x_2)$ which is the autocovariance function of the random field $R(x,\theta)$ defined on the domain Ω. Following Mercer's Theorem, $C(x_1,x_2)$ has the following spectral or eigen-decomposition:

$$C(x_1,x_2) = \sum_{i=1}^{\infty}\lambda_i\phi_i(x_1)\phi_i(x_2) \tag{6}$$

and its eigenvalues and eigenfunctions can be obtained by means of the homogeneous Fredholm integral equation:

$$\int_{\Omega} C(x_1, x_2) \phi_i(x_1) dx_1 = \lambda_i \phi_i(x_2) \tag{7}$$

By virtue of combination between random field and interval uncertainty for the constitutive matrix, based on the standard potential energy of finite element method [15], the potential energy in a linearly elastic body under consideration of unit thickness is represented in a hybrid mathematical model as:

$$
\begin{aligned}
\Pi_p &= \sum_{e=1}^{A_e} \int_{\Omega^e} \frac{1}{2} \left(\varepsilon_e^I(\theta)\right)^T D\left(E(x,\theta), \nu^I\right) \varepsilon_e^I(\theta) d\Omega^e - \sum_{e=1}^{A_e} \int_{S^e} \left(u_e^I(x,\theta)\right)^T \{q_e^I\} dS^e \\
&= \sum_{e=1}^{A_e} \int_{\Omega^e} \frac{1}{2} \left(U_e^I(\theta)\right)^T B^T D\left(E(x,\theta), \nu^I\right) B U_e^I(\theta) d\Omega^e - \sum_{e=1}^{A_e} \int_{S^e} \left(u_e^I(x,\theta)\right)^T \{q_e^I\} dS^e \\
&= \sum_{e=1}^{A_e} \frac{1}{2} \left(U_e^I(\theta)\right)^T k_e^I(\theta) U_e^I(\theta) - \sum_{e=1}^{A_e} \left(U_e^I(\theta)\right)^T \{F_e^I\}
\end{aligned}
\tag{8}
$$

where $u_e^I(\theta, x)$, $U_e^I(\theta)$, $U^I(\theta)$, $\varepsilon_e^I(\theta)$, and $\{q_e^I\}$ are accordingly the interval random displacement field of elements, interval random nodal displacements of elements, interval random nodal displacements of structure in global coordinate system, interval random strain field, and interval surface tractions; A_e, Ω^e, S^e are the number of elements associated with the discretization, domain of the element, surface area of interval surface tractions exerted on the element in that order; the interval nodal forces of elements, approximated by the interval surface tractions are symbolized as:

$$\{F_e^I\} = \int_{S^e} [N]^T \{q_e^I\} dS^e \tag{9}$$

where $[N]$ is the shape function matrix. The stiffness matrix of the eth element is an interval random matrix and can be expressed as:

$$
\begin{aligned}
k_e^I(\theta) &= \int_{\Omega^e} B^T D\left(E(x,\theta), \nu^I\right) B d\Omega^e \\
&= \int_{\Omega^e} B^T D_0\left(E_0, \nu^I\right) B \cdot d\Omega^e + \sum_{i=1}^{\infty} \int_{\Omega^e} \sqrt{\lambda_i} \phi_i(x) \cdot B^T D_0\left(E_0, \nu^I\right) B.\xi_i(\theta) \cdot d\Omega^e \\
&= \int_{\Omega^e} B^T E_0 Q(\nu^I) B \cdot d\Omega^e + \sum_{i=1}^{\infty} \xi_i(\theta) \int_{\Omega^e} \omega_i(x) \cdot B^T E_0 Q(\nu^I) B \cdot d\Omega^e \\
&= k_{e0}^I + \sum_{i=1}^{\infty} k_{ei}^I \xi_i(\theta)
\end{aligned}
\tag{10}
$$

where $D_0\left(E_0, \nu^I\right)$ is the interval constitutive matrix corresponding to E_0; $k_{e0}^I = \int_{\Omega^e} B^T E_0 Q(\nu^I) B \cdot d\Omega^e$ is the interval mean stiffness matrix corresponding to the mean value of elastic modulus; $k_{ei}^I = \int_{\Omega^e} \omega_i(x) B^T E_0 Q(\nu^I) B \cdot d\Omega^e$ are the interval stiffness matrices.

By assembling element stiffness matrix, the interval random global stiffness matrix can be expressed as:

$$K^I(\theta) = \sum_{e=1}^{A_e} k_e^I(\theta) = \sum_{e=1}^{A_e} \left(k_{e0}^I + \sum_{i=1}^{\infty} k_{ei}^I \xi_i(\theta) \right) = \sum_{e=1}^{A_e} \sum_{i=0}^{\infty} k_{ei}^I \xi_i(\theta) = \sum_{i=0}^{\infty} K_i^I \xi_i(\theta) \qquad (11)$$

where K_i^I is the assembling of interval stiffness matrix k_{ei}^I and $\xi_0(\theta)$ is assigned to be equal to 1. Eq. (8) takes the form:

$$\Pi_p = \frac{1}{2} \left(U^I(\theta) \right)^T K^I(\theta) U^I(\theta) - \left(U^I(\theta) \right)^T \left\{ F^I \right\} \qquad (12)$$

where
$$\left\{ F^I \right\} = \sum_{e=1}^{A_e} \left\{ F_e^I \right\} \qquad (13)$$

The governing equation of finite element analysis can be obtained by employing the principle of stationary potential energy for Eq. (12):

$$K^I(\theta) U^I(\theta) = F^I \qquad (14)$$

where $F^I = \left\{ F_1^I, \ldots, F_r^I, \ldots \right\}^T$ is the multiple interval vector of applied loads in which F_r^I is the interval variables fixed within the range of $\left[\underline{F}_r, \overline{F}_r \right]$. $\underline{F}_r$ and $\overline{F}_r$ are the lower and upper bounds of F_r^I, respectively. $U^I(\theta)$ is the multiple interval random vector of nodal displacement due to the interval randomness of $K^I(\theta)$ and interval uncertainty of F^I. By expanding the concept of SSFEM, $U^I(\theta)$ can be represented by using stochastic expansion called Polynomial Chaos Expansion (PCE) and interval coefficients:

$$U^I(\theta) = a_0^I \Gamma_0 + \sum_{i_1=1}^{\infty} a_{i_1}^I \Gamma_1 \left(\xi_{i_1}(\theta) \right) + \sum_{i_1=1}^{\infty} \sum_{i_2=1}^{i_1} a_{i_1 i_2}^I \Gamma_2 \left(\xi_{i_1}(\theta), \xi_{i_2}(\theta) \right)$$
$$+ \sum_{i_1=1}^{\infty} \sum_{i_2=1}^{i_1} \sum_{i_3=1}^{i_2} a_{i_1 i_2 i_3}^I \Gamma_3 \left(\xi_{i_1}(\theta), \xi_{i_2}(\theta), \xi_{i_3}(\theta) \right) \qquad (15)$$
$$+ \sum_{i_1=1}^{\infty} \sum_{i_2=1}^{i_1} \sum_{i_3=1}^{i_2} \sum_{i_4=1}^{i_3} a_{i_1 i_2 i_3 i_4}^I \Gamma_4 \left(\xi_{i_1}(\theta), \xi_{i_2}(\theta), \xi_{i_3}(\theta), \xi_{i_4}(\theta) \right) + \ldots$$

where $\left\{\xi_{i_k}(\theta)\right\}_{k=1}^{\infty}$ is a set of Gaussian random variables; $a_0^I, a_{i_1}^I, a_{i_1 i_2}^I, a_{i_1 i_2 i_3}^I, a_{i_1 i_2 i_3 i_4}^I, \ldots$ are interval coefficients in the spirit of proposed framework due to the incorporated interval uncertainty; $\Gamma_p\left(\xi_{i_1}(\theta), \ldots, \xi_{i_p}(\theta)\right)$ is a multidimensional Hermite polynomials of order p of the multidimensional standard Gaussian random variables described as:

$$\Gamma_p\left(\xi_{i_1}(\theta), \ldots, \xi_{i_p}(\theta)\right) = e^{\frac{1}{2}\sum_{k=1}^{p}\xi_{i_k}^2} \prod_{k=1}^{p}\left(-\frac{\partial}{\partial \xi_{i_k}(\theta)}\right) e^{-\frac{1}{2}\sum_{k=1}^{p}\xi_{i_k}^2} \tag{16}$$

Eq. (15) can be rewritten for convenience in terms of notations as:

$$\begin{aligned} U^I(\theta) &= U_0^I \psi_0(\theta) + U_1^I \psi_1(\theta) + U_2^I \psi_2(\theta) + U_3^I \psi_3(\theta) + \cdots \\ &= \sum_{j=0}^{\infty} U_j^I \psi_j(\theta) \end{aligned} \tag{17}$$

where $\left\{\psi_j(\theta)\right\}_{i=1}^{\infty}$ denotes the series of Hermite polynomials comprising a set of random variables $\xi(\theta) = \left\{\xi_i(\theta)\right\}_{i=1}^{\infty}$. $\left\{U_j^I\right\}_{i=1}^{\infty} = \left\{\left[\underline{U}_j^I, \overline{U}_j^I\right]\right\}_{i=1}^{\infty}$ are interval vectors indicating uncertain-but-bounded coefficients corresponding to $\left\{\psi_j(\theta)\right\}_{i=1}^{\infty}$ due to the interval uncertainty accommodated in the hybrid model of uncertainty. $\left\{\psi_j(\theta)\right\}_{i=1}^{\infty}$ is the orthogonal polynomials satisfying:

$$\left\langle \psi_j(\theta), \psi_k(\theta) \right\rangle = \left\langle \psi_k^2(\theta) \right\rangle \delta_{jk} \tag{18}$$

where δ_{jk} is the Kronecker delta and $\langle . \rangle$ denotes the mathematical expression of the inner product in the Hilbert space:

$$\left\langle f(\xi(\theta)), g(\xi(\theta)) \right\rangle = \int f(\xi(\theta)) g(\xi(\theta)) W(\xi(\theta)) d\xi(\theta) \tag{19}$$

where $W(\xi(\theta))$ is the weight function corresponding to the PCE:

$$W(\xi(\theta)) = \frac{1}{\sqrt{(2\pi)^p}} e^{-1/2\xi(\theta)^T \xi(\theta)} \tag{20}$$

Substituting Eqs. (11) and (17) into Eq. (14) yields:

$$\left(\sum_{i=0}^{\infty} K_i^I \xi_i(\theta)\right)\left(\sum_{j=0}^{\infty} U_j^I \psi_j(\theta)\right) = F^I \tag{21}$$

Truncating the K-L expansion after M terms and PCE after P terms and minimizing the residual in the mean square sense to attain the optimal approximation of space spanned by the polynomials $\left\{\psi_j(\theta)\right\}_{i=1}^{P}$ for Eq. (21) yields:

$$\left\langle \sum_{i=0}^{M}\sum_{j=0}^{P}K_i^I U_j^I \xi_i(\theta)\psi_j(\theta),\psi_k(\theta)\right\rangle = \left\langle F^I,\psi_k(\theta)\right\rangle \tag{22}$$

where $k = 0,\ldots, P$; c_{ijk} and F_k^I are given by:

$$c_{ijk} = \left\langle \xi_i(\theta)\psi_j(\theta)\psi_k(\theta)\right\rangle \tag{23}$$

$$F_k^I = \left\langle F^I,\psi_k(\theta)\right\rangle \tag{24}$$

By reorganizing terms, Eq. (22) becomes:

$$\sum_{i=0}^{M}\sum_{j=0}^{P}c_{ijk}K_i^I U_j^I = F_k^I \tag{25}$$

Values of c_{ijk} are available in the tabulated form provided by reference [7] or evaluated methodically in [10]. The number of terms P of PCE is a function evaluated by the number of terms M and the polynomial order p:

$$P = \sum_{i_p=1}^{p}\frac{\left(M+i_p-1\right)!}{i_p!\left(M-1\right)!} \tag{26}$$

As discussed previously, ISSFEM will yield interval values for the statistics of system responses. Once the U_j^I in Eq. (22) is addressed, the interval statistic values of random interval responses, namely, interval mean value and interval covariance matrix of displacements can be obtained as:

$$E\left[U^I(\theta)\right] = \sum_{j=0}^{P}\left\langle U_j^I\psi_j(\theta)\right\rangle = U_0^I \tag{27}$$

$$\begin{aligned}\mathrm{Cov}\left[U^I(\theta),U^I(\theta)\right] &= \left\langle \left(U^I(\theta)-U_0^I\right)\otimes\left(U^I(\theta)-U_0^I\right)\right\rangle \\ &= \left\langle \left(\sum_{j=0}^{P}U_j^I\psi_j(\theta)-U_0^I\right)\otimes\left(\sum_{j=0}^{P}U_j^I\psi_j(\theta)-U_0^I\right)\right\rangle \\ &= \sum_{i=1}^{P}\left\langle \psi_i^2\right\rangle U_j^I\otimes U_j^I\end{aligned} \tag{28}$$

where $\otimes$ is outer (tensor) product. The interval random strain and stress at a location x within the element of structure under consideration are given by means of PCE:

$$\varepsilon^{I}(x,\theta) = \sum_{j=0}^{P} \psi_{j}(\theta)\varepsilon_{j}^{I}(x) \tag{29}$$

$$\begin{aligned}\sigma^{I}(x,\theta) &= D^{I}(x,\theta)\varepsilon_{j}^{I}(x) \\ &= \sum_{i=0}^{M}\sum_{j=0}^{P}\xi_{i}(\theta)\psi_{j}(\theta)D_{i}^{I}(x)\varepsilon_{j}^{I}(x)\end{aligned} \tag{30}$$

where $\varepsilon_{j}^{I}(x) = B^{T}\{U_{j}^{I}\}^{e}$ is the interval strain vector at a location x inside the considered element derived from the vector comprising interval nodal displacement of that element. $D_{i}^{I}(x) = \sqrt{\lambda_{i}}\phi_{i}(x)D_{0}(E_{0},v^{I})$ is the interval constitutive matrix with notation $D_{0}^{I}(x) = D_{0}(E_{0},v^{I})$. Defining $\sigma_{ij}^{I}(x) = D_{i}^{I}(x)\varepsilon_{j}^{I}(x)$, the interval mean value and interval covariance matrix of stress can be derived as [17]:

$$E\left[\sigma^{I}(x,\theta)\right] = \sum_{i=0}^{M}\sum_{j=0}^{P}\left\langle\xi_{i}(\theta)\psi_{j}(\theta)\right\rangle\sigma_{ij}^{I}(x) = \sum_{i=0}^{M}\sigma_{ii}^{I}(x) \tag{31}$$

$$\begin{aligned}Cov\left[\sigma^{I}(x,\theta),\sigma^{I}(x,\theta)\right] &= \sum_{k=0}^{P}\sum_{j=0}^{P}\sum_{l=0}^{M}\sum_{i=0}^{M}c_{iljk}\sigma_{ij}(x)\otimes\sigma_{lk}(x) \\ &\quad - E\left[\sigma^{I}(x,\theta)\right]\otimes E\left[\sigma^{I}(x,\theta)\right]\end{aligned} \tag{32}$$

where $c_{iljk} = \left\langle\xi_{i}(\theta)\xi_{l}(\theta)\psi_{j}(\theta)\psi_{k}(\theta)\right\rangle$ can be solved analogously as [17]

Following that, the interval standard deviation of displacements and stresses, symbolized as $Std\left[U^{I}(\theta)\right]$ and $Std\left[\sigma^{I}(x,\theta)\right]$, can be attained straightforwardly evaluated based on their covariance matrices.

The general evaluation of change ranges for these responses can be solved by means of interval analysis incorporated in spectral stochastic finite element analysis. Thus, the response variability is correspondingly addressed by the bounds of mean and standard deviation of the output variable followed by extending the procedure of SSFEM in the spirit of interval analysis. Even, in general, a dual approach is possible where the uncertain response is expressed by the mean and standard deviation of the interval bounds for mixed interval probabilistic model, it is quite difficult to consider comparative study between two approaches. Admittedly, the range evaluated by bound of mean of the stochastic output can be identical as that determined by mean of interval bounds as mentioned in [58]. However,

the comparative study relating to the bound of the output variable from two approaches are questionable for variance values when computing variance for interval data is NP-Hard variance [59] and the solution procedure of the responses is more intricate for problems in the presence of random field parameters. In the future, the comparative study for these approaches will be investigated to clarify this consideration.

In general, the aim of interval analysis is similar to that of the optimization problem as its objective is to find the potential enclosure for the output corresponding to input parameters changing within fixed ranges restricted by upper and lower confines. Therefore, interval analysis can be transformed into optimization problems. In this paper, the randomized low-discrepancy sequences initialized particles and high-order nonlinear inertia weight, denoted as RLHNPSO [45] is adopted to handle the interval analysis embedded into ISSFEM. This implementation is presented in the next section.

As aforementioned, the statistical moments of the interval random responses produced by ISSFEM are intervals. Therefore, the probability density function (PDF) and cumulative distribution function (CDF) of the random interval response $R_{res}^{I}(\theta)$ (displacements or stresses) are formed in bounding functions, respectively. These statistical functions can be appropriately visualized by means of random sampling generator based on the polynomial chaos expansion (PCE) in terms of the random interval response $R_{res}^{I}(\theta)$, denoted as the PCE-R (see Eq. 17 for displacements or Eq. 30 for stresses), whose uncertain-but-bounded coefficients are influenced by the interval input parameters. For any arbitrary collection within prescribed constraints of input parameters, corresponding statistical moments of the interval random responses $R_{res}^{I}(\theta)$ and equivalent coefficients of the PCE-R and are accessibly specified. In the scope of this paper, due to advantages in expressing probability theory in terms of expectations, bounds of PDF $f_{\mathrm{E}^{\mathrm{I}}}\left(R_{res}^{I}(\theta)\right)$ and CDF $F_{\mathrm{E}^{\mathrm{I}}}\left(R_{res}^{I}(\theta)\right)$ are produced by PCE-R. The coefficients of PCE-R are determined based on the expectation of the interval random response $R_{res}^{I}(\theta)$ wherein the lower and upper bounds are respectively symbolized as $\underline{\mathrm{E}}\left(R_{res}^{I}(\theta)\right)$ and $\overline{\mathrm{E}}\left(R_{res}^{I}(\theta)\right)$.

Suppose that the interval random response $R_{res}^{I}(\theta)$ is defined on a sample-space Ω and its information is represented via the interval-valued expectation. The interval-valued expectation can be denoted as function $G(R_{res}^{I}(\theta))$ in which G( ) is the mapping expectation function regarding uncertainty parameters of the input and interval random response $R_{res}^{I}(\theta)$. Thus, the bounds of the interval-valued expectation $\mathrm{E}^{\mathrm{I}}\left(R_{res}^{I}(\theta)\right)$ can be generally expressed as the following:

$$\underline{\mathrm{E}}\left(R_{res}^{I}(\theta)\right) = \min G\left(R_{res}^{I}(\theta)\right) \tag{33}$$

$$\bar{E}\left(R_{res}^{I}(\theta)\right) = \max G\left(R_{res}^{I}(\theta)\right) \tag{34}$$

These interval-valued expectations can be effectively specified by proposed framework, to be more detailed, see Eq. 27 for displacement or Eq. 31 for stress. Bounding functions of PDF and CDF of the random interval responses $R_{res}^{I}(\theta)$ are straightforwardly denoted for the convenience as the following

$$f_{E^I}\left(R_{res}^{I}(\theta)\right) = \left[f_{\underline{E}}\left(R_{res}^{I}(\theta)\right), f_{\bar{E}}\left(R_{res}^{I}(\theta)\right) \right] \tag{35}$$

$$F_{E^I}\left(R_{res}^{I}(\theta)\right) = \left[F_{\underline{E}}\left(R_{res}^{I}(\theta)\right), F_{\bar{E}}\left(R_{res}^{I}(\theta)\right) \right] \tag{36}$$

where $f_{\underline{E}}\left(R_{res}^{I}(\theta)\right)$ and $f_{\bar{E}}\left(R_{res}^{I}(\theta)\right)$ indicating the PDFs of the random interval responses $R_{res}^{I}(\theta)$ are consistent with the case in which $E^I\left(R_{res}^{I}(\theta)\right)$ attain its lower bound $\underline{E}\left(R_{res}^{I}(\theta)\right)$ and upper bound $\bar{E}\left(R_{res}^{I}(\theta)\right)$. $F_{\underline{E}}\left(R_{res}^{I}(\theta)\right)$ and $F_{\bar{E}}\left(R_{res}^{I}(\theta)\right)$ indicating the CDFs of the random interval responses $R_{res}^{I}(\theta)$ are consistent with the case in which $E^I\left(R_{res}^{I}(\theta)\right)$ attain its lower bound $\underline{E}\left(R_{res}^{I}(\theta)\right)$ and upper bound $\bar{E}\left(R_{res}^{I}(\theta)\right)$.

3. SOLVING STRATEGY OF ISSFEM

The investigation of structural responses for a complex structure under consideration of uncertainty attracts widespread interests due to its complexity [60]. Predicting output response is to examine how the solutions move among their possible ranges. Identifying and displaying the uncertainties on the outputs using the Monte Carlo Simulation is widely recognised in structural analysis [61]. However, this sampling method cannot lead to optimal solutions with respect to using random pseudo generator as it may provide the change ranges for the output with error [62]. Additionally, the computational expense is much more required corresponding to the increasing number of iterations to search the appropriate solutions for the output. Therefore, the endeavour to mitigate these issues by searching any alternatives for uncertainty analysis is considered. The problem investigated herein, interval quantification is incorporated in stochastic mathematics in the context of ISSFEM to address uncertainty problems with respect to different model of uncertainty based on available information of system. The statistical characteristics of responses such as mean and variance in ISSFEM are intervals. Aforementioned, these intervals can be determined by using optimizations:

$$\textit{Find} \qquad \underline{R}_{res}(\theta), \overline{R}_{res}(\theta) \qquad \textit{with} \qquad x^I = \left\{ x_1^I, x_2^I, ..., x_{L_d}^I \right\}$$

$$\underline{x}_1 \le x_1^I \le \overline{x}_1$$
$$\vdots$$
$$\textit{Subject to} \qquad \underline{x}_d \le x_d^I \le \overline{x}_d \qquad \left(d = 1, ..., L_d \right)$$
$$\vdots$$
$$\underline{x}_{L_d} \le x_{L_d}^I \le \overline{x}_{L_d}$$

(37)

where the upper and lower bounds of x_i^I are designated by $\overline{x}_i$ and $\underline{x}_i$, respectively. $\overline{R}_{res}(\theta)$ and $\underline{R}_{res}(\theta)$ are correspondingly the upper and lower bounds of the interval random response variable $R_{res}^I(\theta)$ (displacements or stresses) in the ISSFEM. L_d is the dimension of multiple interval vector X. In this paper, an improved particle swarm optimization, namely, RLHNPSO is adopted to address the interval stochastic problem in ISSFEM.

The traditional particle swarm optimization algorithm was proposed by Kennedy and Eberhart [55]. This algorithm is initialized with a set including population of random solutions called particles. Each particle flies with time in a multidimensional design space with respect to fitness problem to search its optimal position via adjusting its position and velocity simultaneously. The velocity vector is updated based on its own experience as well as experience of other particles. Thus, each particle takes advantages of the social behaviour of population in which promising areas of search space is gained to target better positions as time passes. The effectiveness of PSO has been recently proved on structural optimization problems and its improvements have been studies by many researchers to strengthen the performance for the output [63-66]. Recently, initialization of particle swarms with regard to the application of low-discrepancy sequences have been considering to improve the performance of PSO in the mathematical view [67, 68]. These works showed the efficiency of PSO concerning initial swarms generated by randomised low-discrepancy sequences, namely randomised Sobol sequence. Liu et al. [69] adopted an improved novel PSO algorithm, namely low-discrepancy sequences initialized high-order nonlinear particle swarm optimization (LHNPSO) in the interval problem, but the structure was modelled as a simple beam. Inspired by above studies, in this paper, a variation of LHNPSO with particles initialized by randomised Sobol sequence, denoted as RLHNPSO [45], is employed to implement the interval stochastic analysis in ISSFEM.

A set of initial population in RLHNPSO is defined as

$$X = \left\{ x_{ip} \right\}^T = \left\{ \begin{array}{c} x_1 \\ x_2 \\ \vdots \\ x_{np} \end{array} \right\} \qquad \left(ip = 1, ..., np \right)$$

(38)

where x_{ip} is any particle of the population X generated from the multiple interval vector x^I of ISSFEM problem and np is the number of particles considered in RLHNPSO.

The interval applied loads and Poisson's ratio considered in this study are described by a multiple interval vector x^I in the context of ISSFEM as:

$$x^I = \left\{ F_1^I, \ldots, F_r^I, \ldots, F_R^I, v_1^I, \ldots, v_s^I, \ldots, v_S^I \right\} \tag{39}$$

where $\left\{ F_r^I \right\}_{r=1}^R$ and $\left\{ v_s^I \right\}_{s=1}^S$ are sets including interval variables of applied loads and Poisson's ratio, correspondingly. x^I can be generally defined as $x^I = \left\{ x_1^I, \ldots, x_d^I, \ldots, x_{L_d}^I \right\}$ where L_d is the dimension of x^I and any particle x_{ip} is described as $x_{ip} = \left\{ x_1, \ldots, x_d, \ldots, x_{L_d} \right\}$ generated from x^I.

Each particle is adjusted via its position and velocity. The velocity and position updating rule is given as:

$$v(t+1) = w(t+1)v(t) + c_1 r_1 \left(x_{ip}^{Pb}(t) - x_{ip}(t) \right) + c_2 r_2 \left(x_{ip}^{Gb}(t) - x_{ip}(t) \right) \tag{40}$$

$$x_{ip}(t+1) = x_{ip}(t) + v_{ip}(t+1) \tag{41}$$

where $v_d(t)$, $x_d(t)$, x_{ip}^{Pb} and x_{ip}^{Gb} denote correspondingly the velocity, position, local best ever position and the global best ever position of particle ip^{th} in iteration t^{th}. c_1 and c_2, named as cognitive parameter and social parameter, respectively. They are the acceleration coefficients indicating the degree of directing to the better positions of particles. Constraint of c_1 and c_2 is specified as $0 < c_1 + c_2 < 4$, regularly $c_1 = c_2 = 2$ [64]. r_1 and r_2 indicate random numbers ranging between 0 and 1. w termed as time varying inertial weight controls the search capacities of the swarm. A high-order nonlinear time-varying inertia weight has been recently employed to attain the faster convergence [69]:

$$w(t+1) = w_{\max} - \left(w_{\max} - w_{\min} \right) \left(\frac{t}{T_t} \right)^{1/\pi^2} \tag{42}$$

where $w_{\max} = 0.95$, $w_{\min} = 0.5$ and T_t is the number of iterations for RLHNPSO. The fitness functions of RLHNPSO in the context of ISSFEM are, for instance, the interval mean value or interval standard deviation of responses and the lower and upper bounds of these functions are respectively the minimum and maximum values of the problems under consideration. The general solving strategy of ISSFEM with the incorporation of the algorithm RLHNPSO is stated in Figure 1:

Interval variables

F^I, ν^I

Random field

$E(x, \theta)$

Input

RLHNPSO for ISSFEM

$$x^I = \left\{ F_1^I, \ldots, F_r^I, \ldots, F_R^I, \nu_1^I, \ldots, \nu_s^I, \ldots, \nu_S^I \right\}$$

$$E(x, \theta) = E_0 \left(1 + R(x, \theta) \right)$$

$$\sum_{i=0}^{M} \sum_{j=0}^{P} c_{ijk} K_i^I U_j^I = F_k^I, \quad k = 0, \ldots, P$$

Fitness function

$$E\left[U^I(\theta) \right]$$

or $\quad E\left[\sigma^I(x, \theta) \right]$

or $\quad Std\left[U^I(\theta) \right]$

or $\quad Std\left[\sigma^I(x, \theta) \right]$

Evaluate the fitness function

Bounds for interval random responses
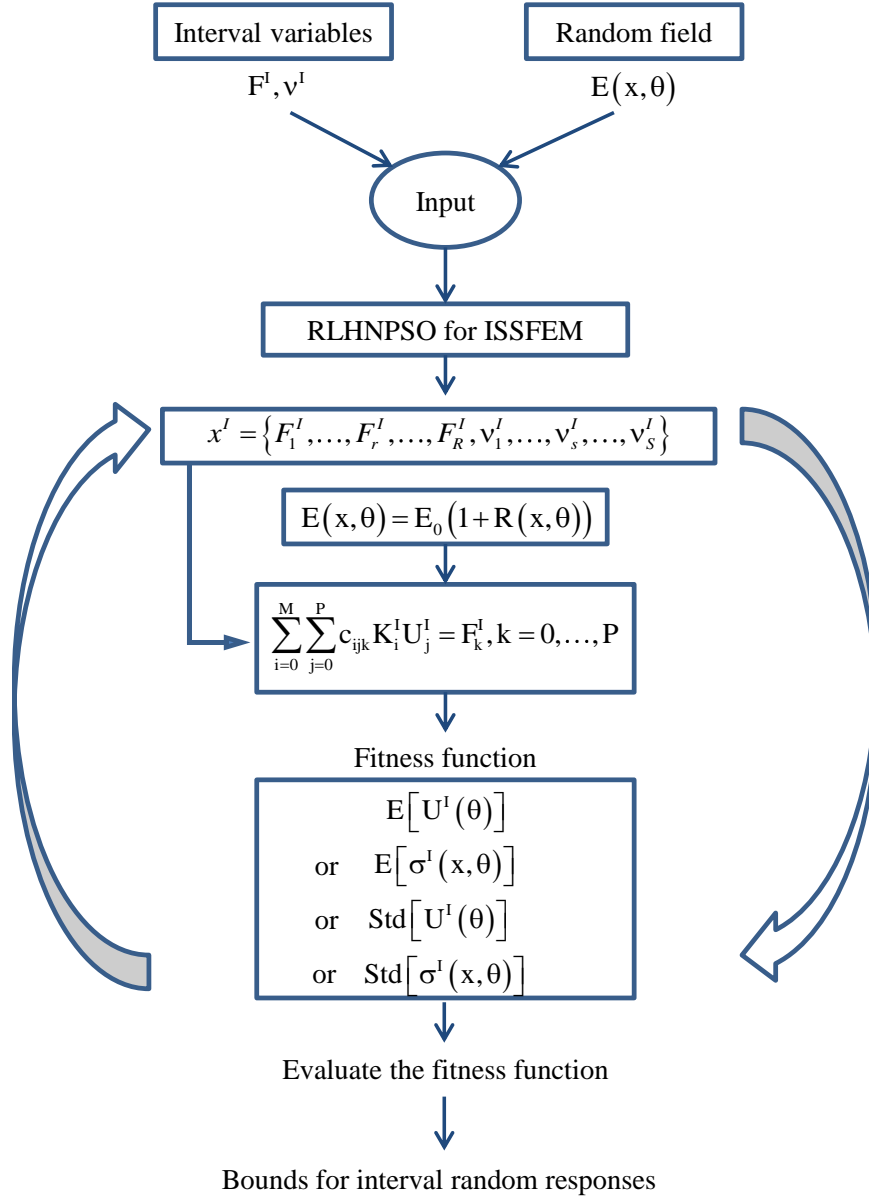
Figure 1. The incorporation of the algorithm RLHNPSO in ISSFEM

4. NUMERICAL EXAMPLES

In this section three numerical tests in consideration of plane stress analysis for plates with unit thickness are performed using the algorithm RLHNPSO presented in the previous section to capture the bounds for the numerical characteristics of the interval random responses of ISSFEM. Different cases from two-dimensional solid structures are examined into the increasing level of uncertainty to show the efficiency of the approach developed in this paper. The accuracy of the results obtained by the presented method is verified by the randomised Quasi-Monte Carlo simulation method (RQMCSM).

The sources of uncertainty comprise the elastic modulus, Poisson's ratio and applied forces. The elastic modulus is modelled as a Gaussian random field while Poisson's ratio and applied forces are considered as interval variables. The mean value for elastic modulus is set as 21e4 *MPA*. A commonly exponential function is employed to describe the covariance function for spatially varying random field of elastic modulus:

$$C_E\left(x_1, x_2\right) = \sigma^2 \exp\left(-\frac{|x_1 - x_2|}{L_{cx}} - \frac{|y_1 - y_2|}{L_{cy}}\right) \tag{43}$$

where σ, L_{cx} and L_{cy} are the standard deviation, correlation length in x-direction and correlation length in y-direction, respectively. A closed-form representation of the eigenvalues and eigenfunctions of this covariance function is given in [7, 70]. Four terms in KL expansion and 3rd order in PCE are considered for the test cases.

In this study, 10 particles are initialized and 40 iterations are carried out to attain the solutions of the considered problems, that is, the bounds of mean value and standard deviation of interval random displacements. The number of iterations is considered to avoid the premature convergence for numerical problems. Solutions derived from RLHNPSO are verified by the randomized Quasi-Monte Carlo Simulation (RQMCS) using 10000 iterations.

4.1. Test case 1

Geometry of the L-shape plate subjected to interval forces and its meshing are shown in Figure 2. The domain of plate is discretised over a mesh with 156 nodes and 266 triangular elements. The elements 1, 2 and 3 are noted to be considered for stress evaluation. The covariance function for elastic modulus of this plate is given in Eq. (43) with $L_{cx} = L_{cy} = 1$ (m) and the coefficient of variation of 0.1. A sample realization showing the spatial variations of random field is given in Figure 3. The Poisson's ratio for the whole plate is considered as an interval variable with change range defined as $v^I = [0.27, 0.3]$. The interval vector under consideration for this test case is $x^I = \left\{q_1^I, q_2^I, v^I\right\}$. Deterministic values of q_1^I and q_2^I are 80 N/mm^2 and 60 N/mm^2 while their interval change ratios are accordingly 0.1 and 0.2, respectively. The comparison between RLHNPSO and RQMCS for the mean value and standard deviation of displacements at node A, B and C are carried out to test the performance of RLHNPSO, as shown in Table I while consideration for stresses at some elements is mentioned in Table II. The convergence history of RLHNPSO for the displacements at point A in X direction and at point B in Y direction are illustrated in Figures 4 and 5, respectively and that for σ_y of element 3 is Figure 6. The deformed shape of the plate using the system parameters corresponding to the lower and upper mean value of

displacement at point A in X direction and at point C in Y direction are accordingly plotted in Figures 7 and 8. The convergence history of stress in terms of design variables over iterations is expressed by evaluation of upper bound of mean value of σ_x (MPa) of element 3 as depicted in Figure 9 and mentioned in Table III with truncated iterations. Clearly, this target value starts to converge at iteration 6.

a)   b)
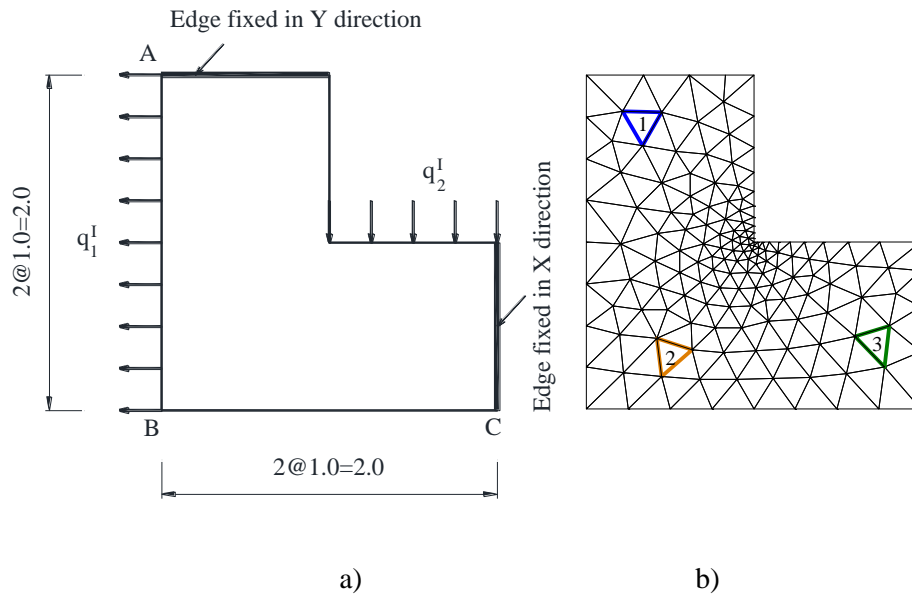
Figure 2. L-shape Plate: (a) geometry of structure; (b) discretization of structure.
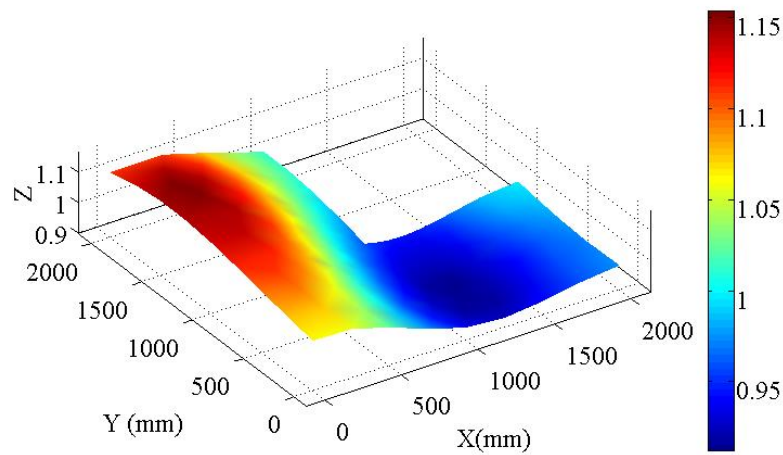
Figure 3. A sample realization of the random field.

From Figures 4 and 5, it can be easily observed that less than 20 iterations of RLHNPSO, in which 10 particles is carried out for each iteration, can produce the convergent solutions which are positively better than the results produced by 10000 Randomized Quasi-Monte Carlo Simulations. Solutions including means and standard deviations from 200 (that is, 10 particles multiplied by 20 iterations) RLHNPSO calculations contain the bounds provided by

10000 RQMCS as shown in Table I. This test case was carried out on a computer equipped with a 3.30 GHz i5-2500 CPU. The time consuming for RLHNPSO including the lower and upper bounds for mean value of displacement in Y direction of node C is 1723.42 seconds while that for RQMCS is 20996.19 seconds which is approximately 12 times in comparison with the former. If the number of iterations of RQMCS or MCS is increased to get better results, more time is required. Figures 7 and 8 show that mean values of interval random responses are intervals, which is different from traditional spectral stochastic finite element analysis.

Table I. Displacements derived from RLHNPSO and QMCS (unit: mm).

Target solutions		Point C (Y direction)		Point A (X direction)	
Methods		RQMCS	RLHNPSO	RQMCS	RLHNPSO
Mean	Upper	0.40632	0.42584	-1.83280	-1.81652
	Lower	-0.92045	-0.93998	-3.13529	-3.14357
Std	Upper	0.06363	0.06468	0.19620	0.19677
	Lower	0.02645	0.02639	0.11767	0.11663
Target solutions		Point B (X direction)		Point B (Y direction)	
Methods		RQMCS	RLHNPSO	RQMCS	RLHNPSO
Mean	Upper	-0.80083	-0.80009	-0.21318	-0.20511
	Lower	-1.14165	-1.14315	-0.53878	-0.54333
Std	Upper	0.08417	0.08444	0.04215	0.04231
	Lower	0.06314	0.06302	0.03004	0.02990

Table II. Stresses derived from RLHNPSO and QMCS (unit: MPa).

Target solutions		σ_x (Element 1)		σ_x (Element 2)	
Methods		RQMCS	RLHNPSO	RQMCS	RLHNPSO
Mean	Upper	-4.87819	-4.01157	91.7659	92.05941
	Lower	-27.6791	-28.28372	48.4949	47.88137
Std	Upper	5.64447	5.74310	19.316	19.35001
	Lower	1.87041	1.75153	12.5187	12.50989
Target solutions		σ_x (Element 3)		σ_y (Element 3)	
Methods		RQMCS	RLHNPSO	RQMCS	RLHNPSO
Mean	Upper	209.336	210.56733	76.4324	77.09375
	Lower	159.95	158.47376	29.1282	28.13896
Std	Upper	42.4623	42.68208	14.8646	14.97038
	Lower	32.8782	32.58080	7.02065	6.85682
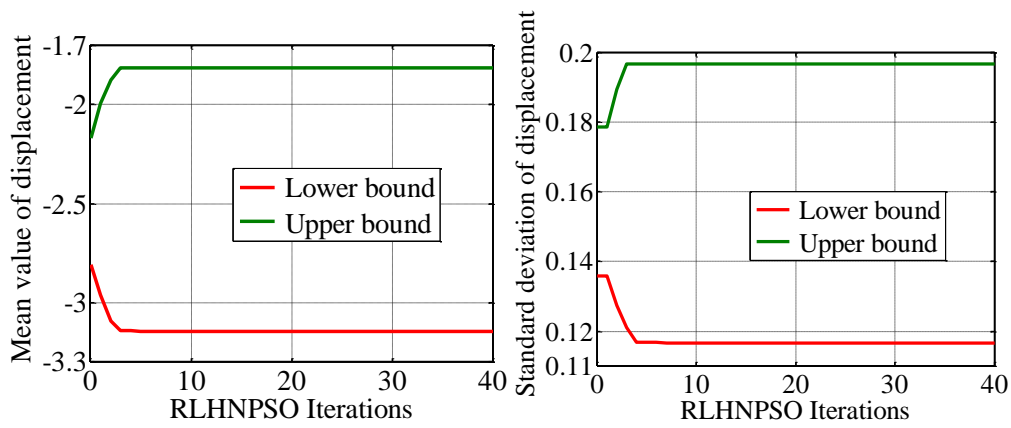
Figure 4. Convergence history of displacement at point A in X direction by means of RLHNPSO. Unit (mm).
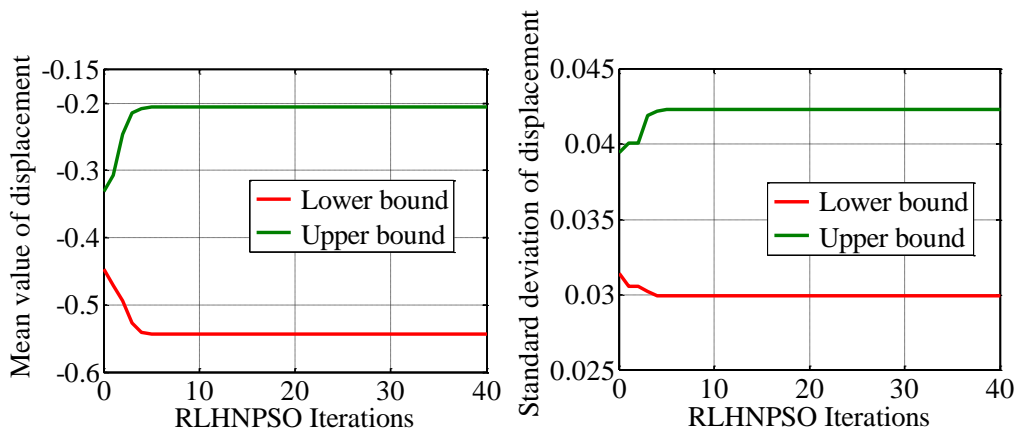
Figure 5. Convergence history of displacement at point B in Y direction by means of RLHNPSO. Unit (mm).
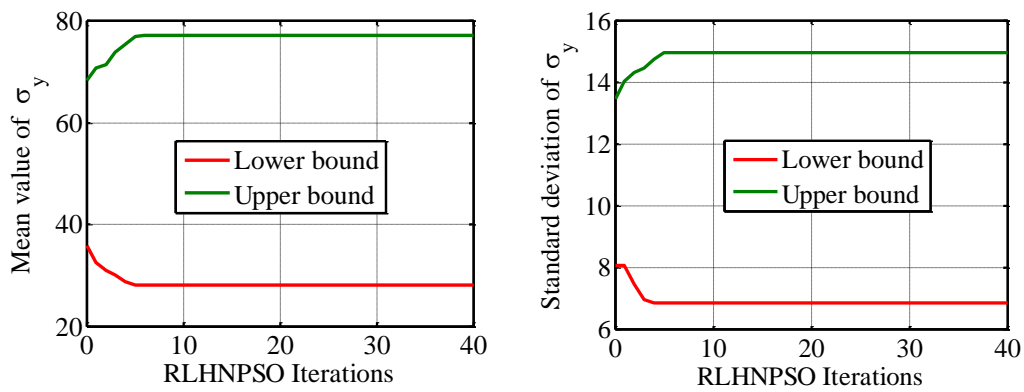
Figure 6. Convergence history of σ_y of element 3 by means of RLHNPSO. Unit (MPa).
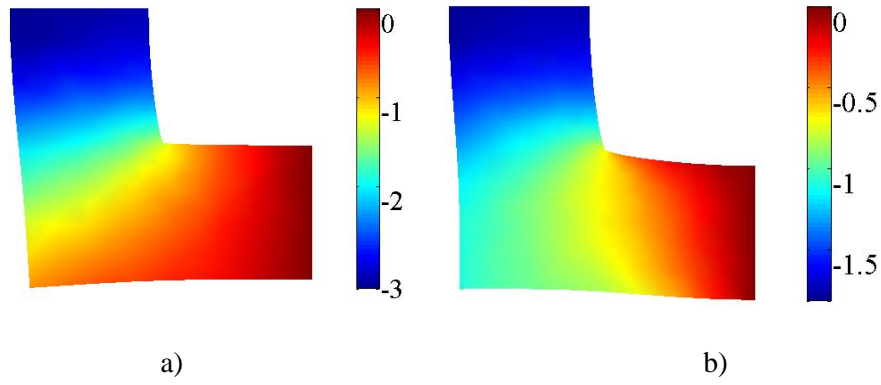
Figure 7. Deformed shape (mm): (a) lower mean value of displacement at A in X direction; (b) upper mean value of displacement at A in X direction.
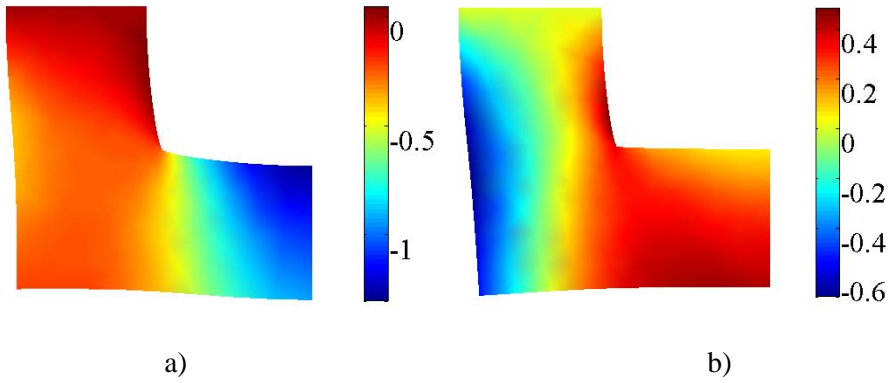
Figure 8. Deformed shape (mm): (a) lower mean value of displacement at C in Y direction; (b) upper mean value of displacement at C in Y direction.

Table III. Upper bound of mean value of σ_x (MPa) of element 3 derived from RLHNPSO based on change range of interval variables, namely q_1^I (N/mm^2), q_2^I (N/mm^2) and ν^I.

Iteration	σ_x	q_1^I	q_2^I	ν^I
	201.93056	-85.52831	-69.59874	0.28544
1	201.93056	-77.75112	-59.85499	0.28858
2	207.63836	-80.95112	-64.65499	0.29458
3	208.91468	-84.15112	-69.45499	0.29275
4	209.84094	-87.35112	-72	0.29468
5	210.56733	-88	-72	0.29772
6	210.56733	-88	-72	0.3
7	210.56733	-88	-72	0.3
8	210.56733	-88	-72	0.3
9	210.56733	-88	-72	0.3
10	210.56733	-88	-72	0.3
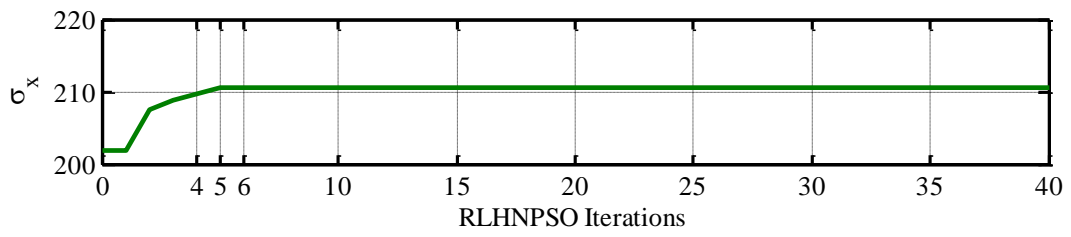
a)
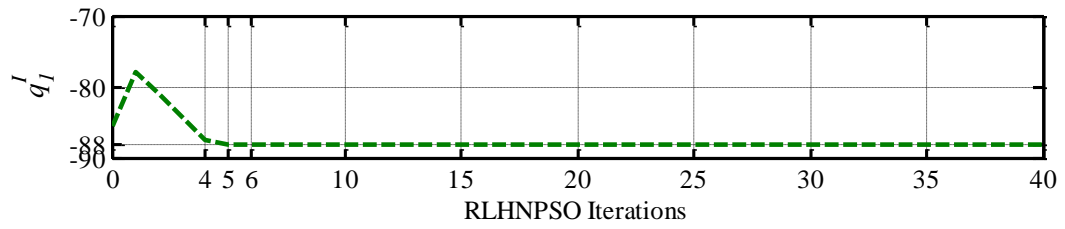
b)
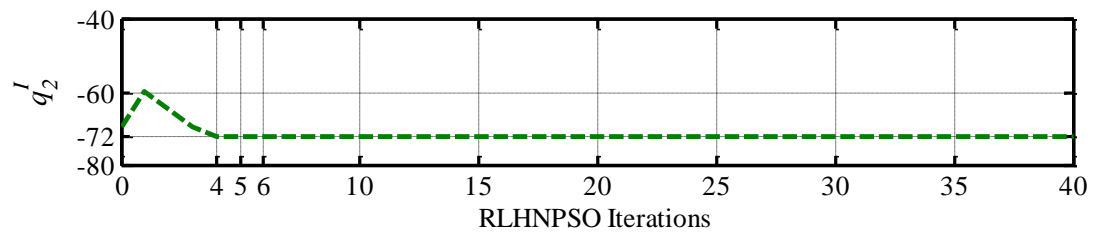
c)
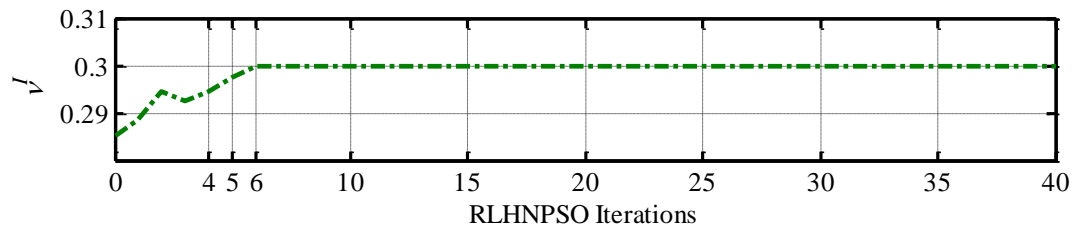
d)

Figure 9. Convergence history of upper bound of mean value of σ_x (MPa) of element 3 by RLHNPSO. Note: q_1^I (N/mm^2), q_2^I (N/mm^2) and σ_x (MPa).

Considering the statistic distribution of the displacement at point A in X direction, let $F1 = F_{\underline{E}}\left(R_{res}^{I}(\theta)\right)$, $F2 = F_{\overline{E}}\left(R_{res}^{I}(\theta)\right)$, $f1 = f_{\underline{E}}\left(R_{res}^{I}(\theta)\right)$ and $f2 = f_{\overline{E}}\left(R_{res}^{I}(\theta)\right)$. The interval coefficients of PCE-R are derived from the implementation of RLHNPSO to investigate the lower and upper bounds of interval-valued expectation of the displacement at point A in X direction. In this work, these bounds are specified by random sampling generator of RQMCS for displacement field presented by polynomial chaos expansion (PCE), known as PCE-R (see section 2). For the purpose of demonstration only, the $f_{E^{I}}\left(R_{res}^{I}(\theta)\right)$ and $F_{E^{I}}(R)$ corresponding to 100,000 samples achieved by using RQMCS for the displacement at point A in X direction are shown in Figures 10 and 11.
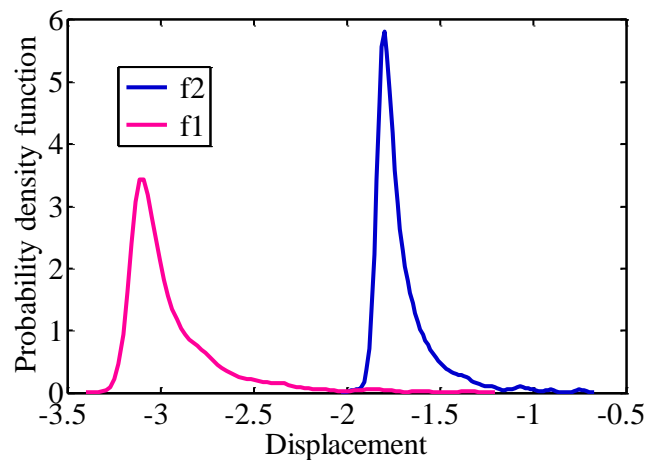
Figure 10. Lower and upper bounds of PDF of displacement at A in X direction (unit: mm).
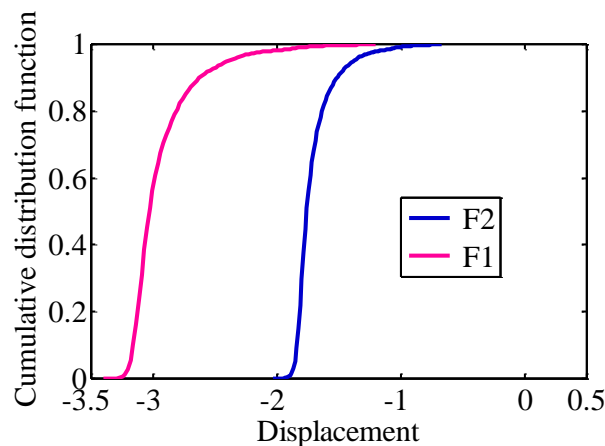
Figure 11. Lower and upper bound of CDF of displacement at A in X direction (unit: mm).

To further test the performance of the RLHNPSO based ISSFEM, the parametric study for the change ranges of response corresponding to different interval change ratios (ICR) is

implemented. The interval change ratios of q_1^I and q_2^I are changing simultaneously for each case while the change range of Poisson's ratio constantly keeps v^I = [0.27, 0.3]. The performance of RLHNPSO is demonstrated in Figures 12 and 13 while some interval mean values and interval standard deviations are collected in Table IV and Table V. Similarly, the performance of RLHNPSO for stresses is shown in Figures 14 and 15. These figures show the wider enclosure of the responses when the interval change ratio is increased. The solutions convergent in the first several iterations even the interval change ratio is 0.3. Tables IV - VII show that the results derived from the RLHNPSO are better those from RQMCS considering the same interval change ratio, that is, solutions obtained from RLHNPSO contain the bounds provided by RQMCS.

Table IV. Intervals of mean value of displacement at C in Y direction (unit: mm).

Interval change ratio	RLHNPSO		RQMCS	
	Lower	Upper	Lower	Upper
0.10	-0.70768	0.19330	-0.69852	0.18134
0.15	-0.92648	0.41349	-0.90486	0.39171
0.20	-1.14527	0.63368	-1.12666	0.62031
0.25	-1.36406	0.85387	-1.34629	0.82933
0.30	-1.58286	1.07406	-1.56859	1.04335

Table V. Intervals of standard deviation of displacement at A in X direction (unit: mm).

Interval change ratio	RLHNPSO		RQMCS	
	Lower	Upper	Lower	Upper
0.1	0.12465	0.18863	0.12512	0.18822
0.15	0.10882	0.20461	0.10975	0.20392
0.2	0.09318	0.22059	0.09386	0.22006
0.25	0.07736	0.23658	0.07840	0.23571
0.3	0.06183	0.25257	0.06317	0.25136
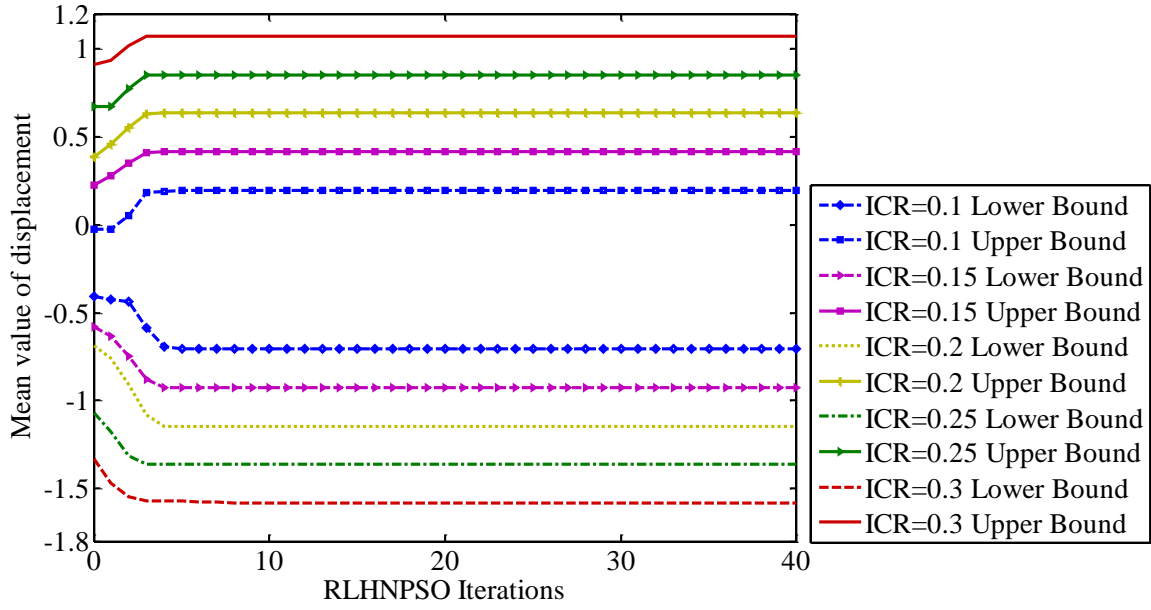
Figure 12. Convergence history of mean of displacement at C in Y direction (unit: mm).
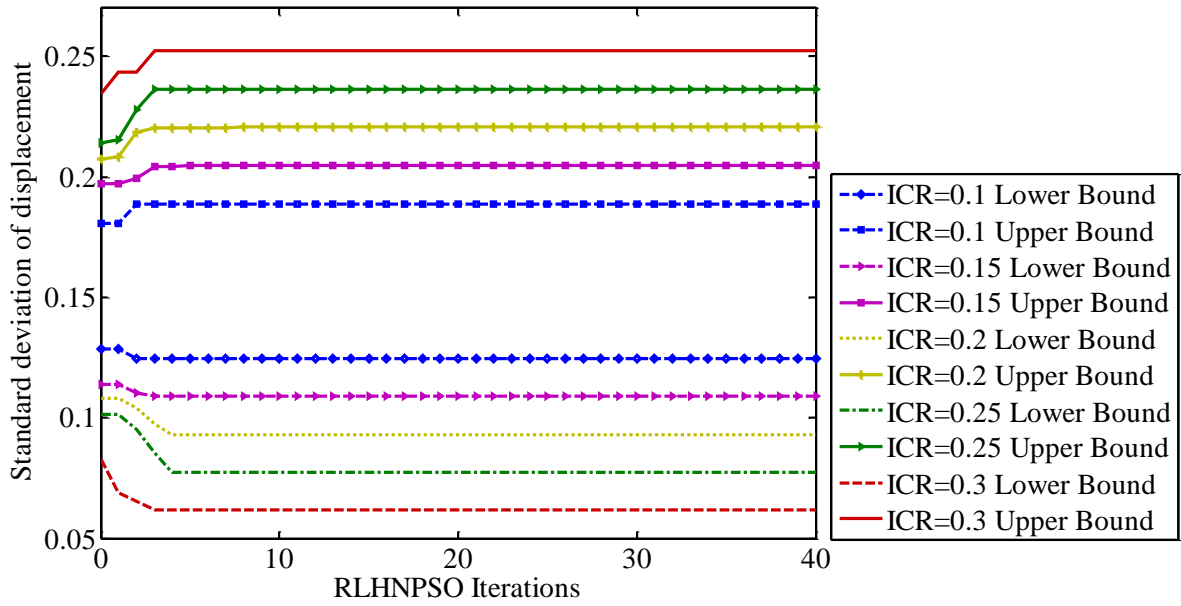
Figure 13. Convergence history of standard deviation of displacement at A in X direction (unit: mm).

Table VI. Intervals of mean value of σ_x of element 80 (unit: MPa).

Interval change ratio	RLHNPSO		RQMCS	
	Lower	Upper	Lower	Upper
0.10	163.871	204.750	164.457	203.804
0.15	154.767	214.057	155.647	213.236
0.20	145.663	223.364	146.847	221.615
0.25	136.559	232.671	138.547	230.918
0.30	127.455	241.978	128.161	240.498

Table VII. Intervals of standard deviation of σ_x of element 80 (unit: MPa).

Interval change ratio	RLHNPSO		RQMCS	
	Lower	Upper	Lower	Upper
0.10	33.4326	41.7567	33.5432	41.5798
0.15	31.5752	43.6547	31.7384	43.5007
0.20	29.7178	45.5528	29.9286	45.2019
0.25	27.8605	47.4508	28.2686	47.0952
0.30	26.0031	49.3488	26.1468	49.0577
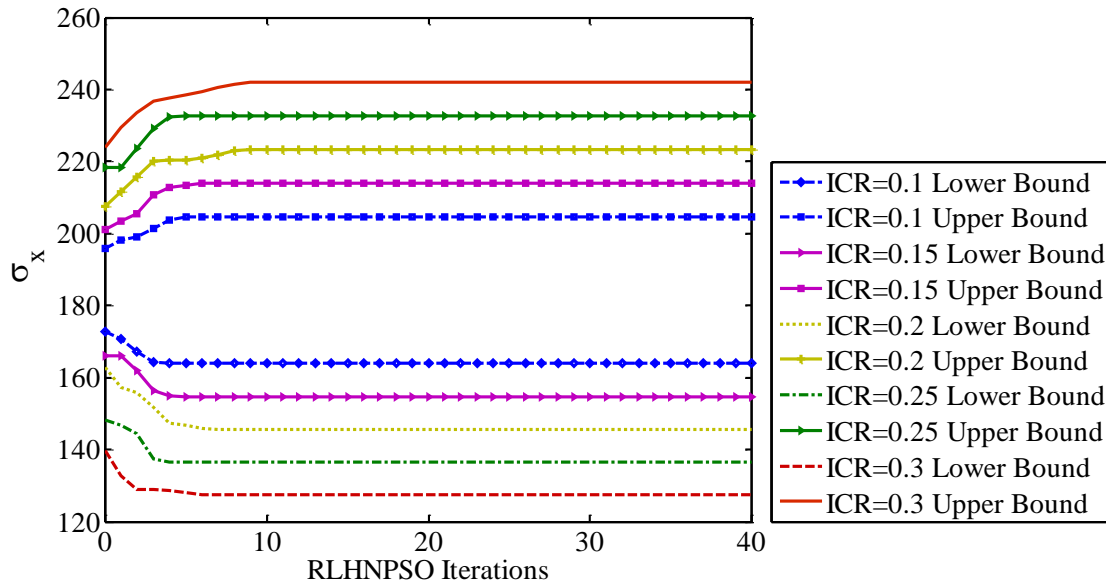
Figure 14. Convergence history of mean of σ_x of element 80 (unit: MPa).
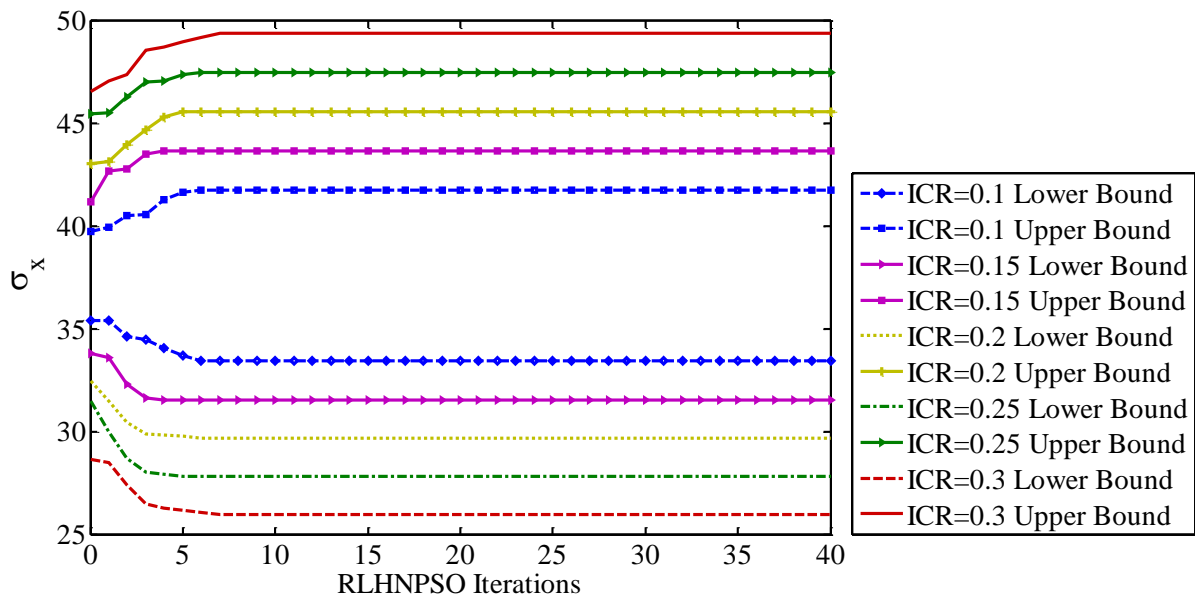
Figure 15. Convergence history of standard deviation of σ_x of element 80 (unit: MPa).

4.2. Test case 2

Dimensions and mesh generation of the plate under interval loads are depicted in Figure 16. The plate is discretised into 198 nodes and 168 four-node quadrilateral elements. The covariance function for elastic modulus of plate is given in Eq. (43) with $L_{cx} = L_{cy} = 0.5$ (m) and the coefficient of variation of 0.15. A sample realization showing the spatial variations of random field is described in Figure 17. The Poisson's ratio of plate is represented by an interval vector consists of three independent interval variables corresponding to the three areas. All the interval Poisson's ratios have the same change range defined as [0.27, 0.3. The multidimensional vector of interval variables under consideration for this test case is $x^I = \{q_1^I, q_2^I, v_1^I, v_2^I, v_3^I\}$. Deterministic values of q_1^I and q_2^I are respectively 40 N/mm^2 and 35 N/mm^2, while their interval change ratios are accordingly 0.2 and 0.3. The comparison between RLHNPSO and RQMCS for the mean value and standard deviation of displacements at node B, C, D and E are carried out to verify the faster convergence of RLHNPSO, as shown in Table VIII. The convergence history of RLHNPSO for the displacements at point B in Y direction and at point E in X direction is described in Figures 18 and 19, respectively.

Admittedly, less than 20 iterations of RLHNPSO, in which 10 particles are considered for each iteration, can produce the convergent solutions which are certainly better than the results produced by 10000 Randomized Quasi-Monte Carlo Simulations. The intervals determined by RLHNPSO contain the bounds produced by 10000 RQMC simulations. The time consuming for RLHNPSO including the lower and upper bounds for mean value of displacement at point C in Y-direction is 2753.21 seconds while RQMCS requires 34045.36 seconds. This test case was carried out on a computer equipped with a 3.30 GHz i5-2500 CPU. The performance of RLHNPSO combined with SSFEM within the framework of ISSFEM is reliable.

a) b)
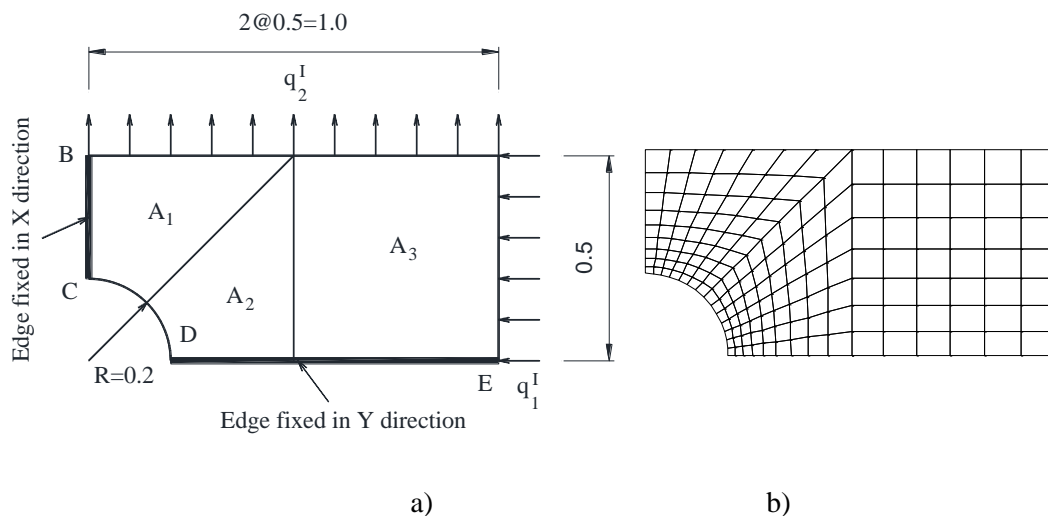
Figure 16. 2D Plate: (a) geometry (unit: m); (b) discretization
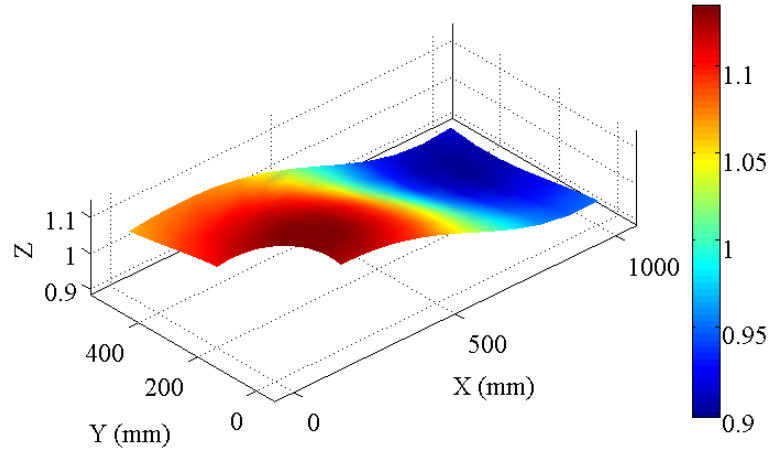
Figure 17. A sample realization of the random field.

Table VIII. Displacements derived from RLHNPSO and QMCS (Unit: mm).

Target solutions		Point B (Y direction)		Point C (Y direction)	
Methods		RQMCS	RLHNPSO	RQMCS	RLHNPSO
Mean	Upper	0.31344	0.31535	0.25851	0.25962
	Lower	0.18099	0.17973	0.14962	0.14929
Std	Upper	0.03761	0.03790	0.03169	0.03182
	Lower	0.02172	0.02157	0.01829	0.01825
Target solutions		Point D (X direction)		Point E (X direction)	
Methods		RQMCS	RLHNPSO	RQMCS	RLHNPSO
Mean	Upper	-0.14846	-0.14781	-0.24430	-0.24232
	Lower	-0.23518	-0.23741	-0.38406	-0.38733
Std	Upper	0.02939	0.02963	0.04044	0.04080
	Lower	0.01849	0.01843	0.02562	0.02540
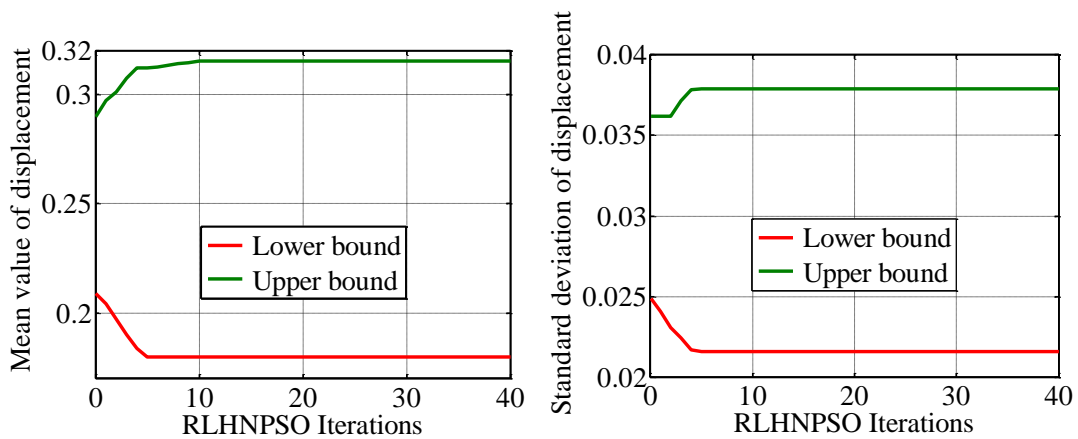
Figure 18. Convergence history of displacement at point B in Y direction (unit: mm).
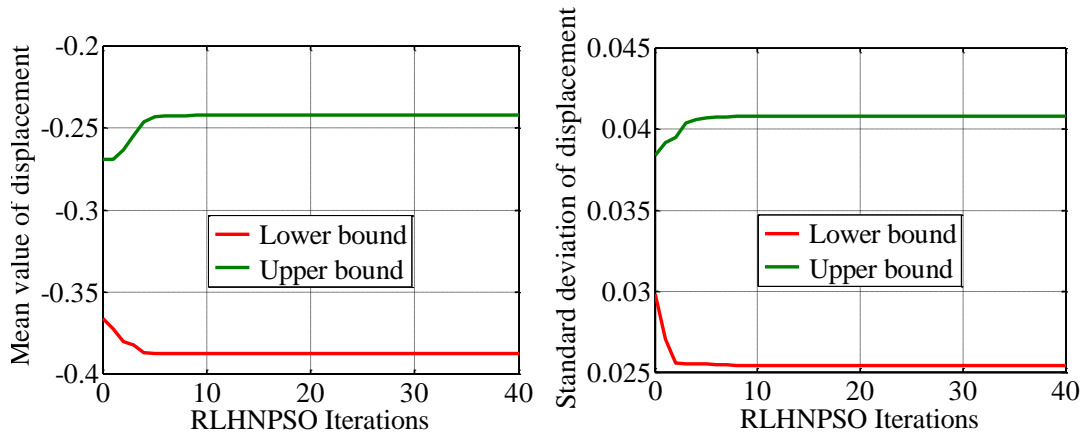
Figure 19. Convergence history of displacement at point E in X direction (unit: mm).

The visualization for bounded mean values of displacement at target point is also shown in this section. The target point considered herein for this issue is the point B. Figure 20 describes the bounded mean values of displacement at point B in Y direction through the two response surfaces of undeformed shape, namely S1 and S2. S1 illustrates the responses of whole plate calculated by using the input parameters which are in accordance with the case of the lower bound mean value of displacement at point B in Y direction determined by means of RLHNPSO. S2 presents the responses surface corresponding to the upper bound mean value of displacement at point B in Y direction by RLHNPSO. It can be seen that the change range of the mean value of the interval random plate response is notable.
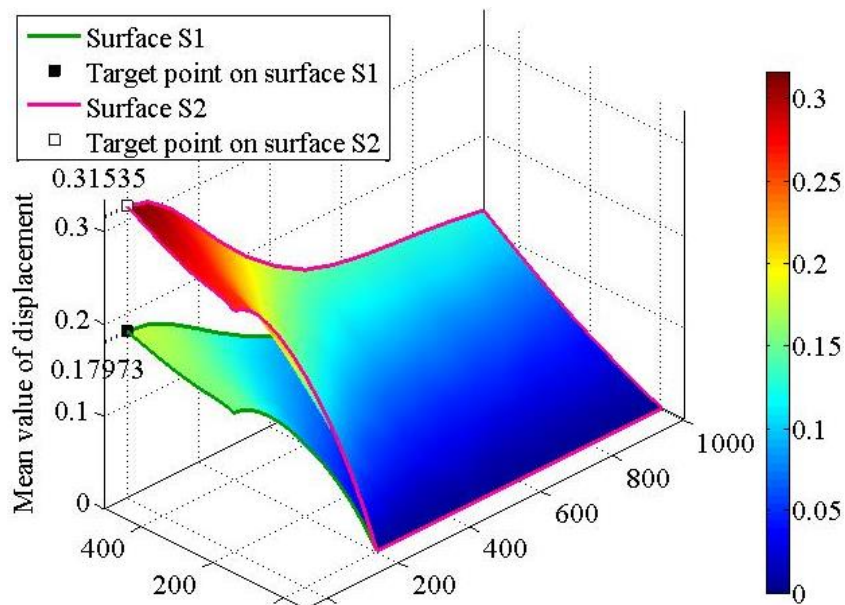
Figure 20. Bounded mean value of displacement at point B in Y direction (unit: mm).

Another issue presented in this test case is the consideration for the distribution of displacement at B in Y direction. The bounding PDF and CDF can be specified using random sampling generator of RQMCS for displacement field presented by polynomial chaos expansion (PCE), known as PCE-*R*. The interval coefficients of PCE-*R* are determined by RQMCS or RLHNPSO, as implemented before with regards to investigation for bounds of $R_{res}^I(\theta)$ and thus produce different bounds for CDF and PDF. Once these coefficients are determined, the bounds for the PDF or CDF of the displacements under consideration can be achieved by using RQMCS with 100,000 samples for each function. Let $F1 = F_{\underline{E}}\left(R_{res}^I(\theta)\right)$, $F2 = F_{\bar{E}}\left(R_{res}^I(\theta)\right)$, $f1 = f_{\underline{E}}\left(R_{res}^I(\theta)\right)$ and $f2 = f_{\bar{E}}\left(R_{res}^I(\theta)\right)$. These bounds are straightforwardly labelled for the convenience as F1 from RLHNPSO, F2 from RLHNPSO, F1 from RQMCS, F2 from RQMCS, f1 from RLHNPSO, f2 from RLHNPSO, f1 from RQMCS, and f2 from RQMCS . Figure 21 shows the comparison between the bounds of probability density derived from RQMCS and those from RLHNPSO while 22 presents the bounds for cumulative distribution. In general, the shape of the probability density and cumulative distributions generated by these two methods are in good agreement in which f1 and f2 from RLHNPSO provide slightly better bounds compared to bounds produced by f1 and f2 from RQMCS. Note in Figure 21 and 22, that the F1, F2, f1 and f2 from RLHNPSO are specified by PCE-R with the case of attaining lower bound of 0.17973 and upper bound of 0.31535 while those from RQMCS produced according to the case of attaining lower bound of 0.18099 and upper bound of 0.31344.
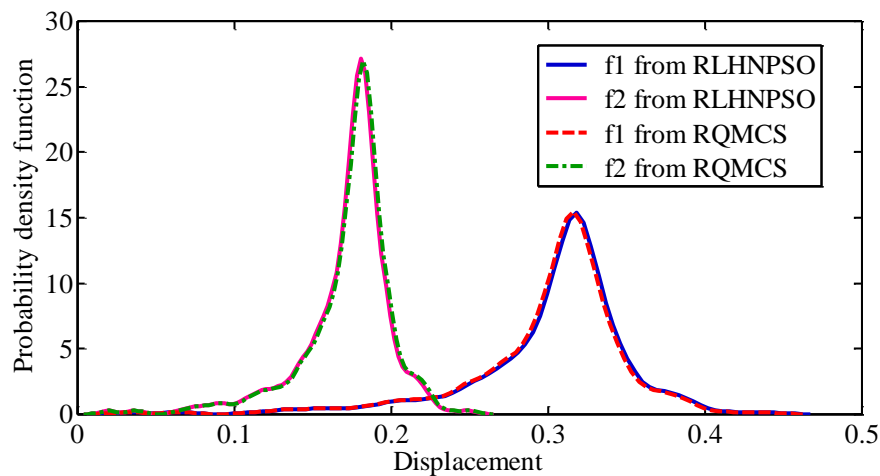

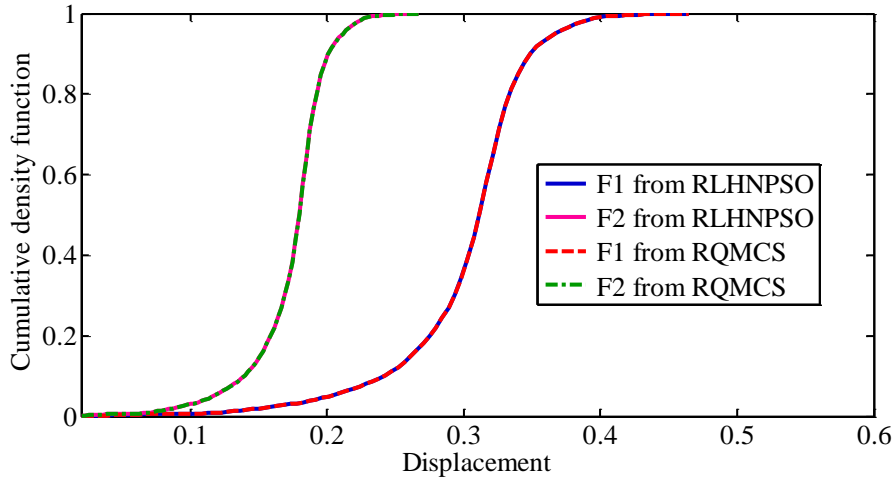Figure 21. Bounds of probability density of displacement at point B in Y direction (unit: mm).

Figure 22. Bonds of cumulative distribution of displacement at point B in Y direction (unit: mm).

Another interest in this section is to do study on variability of mean value and standard deviation of interval random displacement at point E in X direction using RLHNPSO with different interval change ratios. q_1^I and q_2^I have the same interval change ratio for each case while the change range of Poisson's ratio is still specified by $\nu^I = [0.27, 0.3]$. The results shown in Table IX and visualizations depicted in Figures 23 and 24 indicate that the intervals of the statistical moments of interval random response is widening along with the increasing number of interval change ratio.
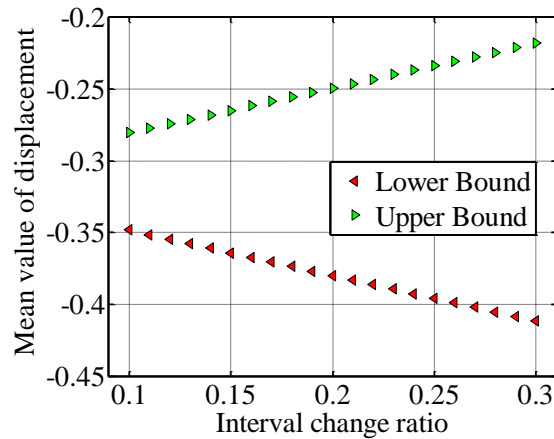
Figure 23. Variability of interval mean of displacement at point E in X direction by RLHNPSO (unit: mm).
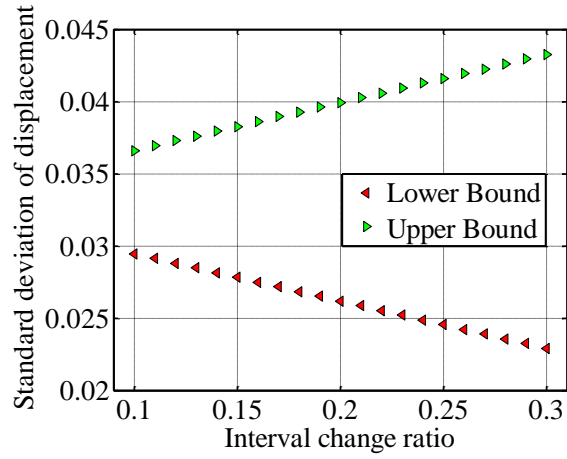
Figure 24. Variability of interval standard deviation of displacement at point E in X direction by RLHNPSO (unit: mm).

Table IX. Interval statistical moments of displacements at point E in X direction (unit: mm).

Interval change ratio	Mean value		Standard deviation	
	Lower	Upper	Lower	Upper
0.10	-0.34827	-0.28038	0.029471	0.036629
0.11	-0.35143	-0.27726	0.029144	0.036961
0.12	-0.3546	-0.27415	0.028816	0.037294
0.13	-0.35777	-0.27103	0.028489	0.037627
0.14	-0.36093	-0.26792	0.028161	0.03796
0.15	-0.3641	-0.2648	0.027834	0.038293
0.16	-0.36726	-0.26168	0.027507	0.038626
0.17	-0.37043	-0.25857	0.027179	0.038959
0.18	-0.3736	-0.25545	0.026852	0.039292
0.19	-0.37676	-0.25234	0.026524	0.039625
0.20	-0.37993	-0.24922	0.026197	0.039958
0.21	-0.38309	-0.24611	0.025869	0.040291
0.22	-0.38626	-0.24299	0.025542	0.040624
0.23	-0.38943	-0.23988	0.025214	0.040957
0.24	-0.39259	-0.23676	0.024887	0.04129
0.25	-0.39576	-0.23365	0.024559	0.041623
0.26	-0.39892	-0.23053	0.024232	0.041956
0.27	-0.40209	-0.22742	0.023904	0.042289
0.28	-0.40526	-0.2243	0.023577	0.042622
0.29	-0.40842	-0.22119	0.02325	0.042955
0.30	-0.41159	-0.21807	0.022922	0.043288

4.3. Test case 3

A square plate with one circle hole subjected to interval loads shown in Figure 26 is under consideration. The domain of the plate is discretised into 192 four-node quadrilateral elements and 224 nodes. The covariance function for elastic modulus of plate given in Eq. (43) with assumption of $L_{cx} = L_{cy} = 0.5$ (m) and the coefficient of variation of 0.2. A sample realization showing the spatial variations of random field is presented in Figure 26.The Poisson's ratio for whole plate is represented by eight independent interval variables $\{v_{ipos}^I\}_{ipos=1}^8$ corresponding to eight areas of the domain $\{A_{ipos}\}_{ipos=1}^8$. All of v_{ipos}^I have the same change range defined as [0.27, 0.3]. The interval vector under consideration for this test case is $x^I = \left\{q_1^I, q_2^I, \{v_{ipos}^I\}_{ipos=1}^8\right\}$. Deterministic values of q_1^I and q_2^I are 80 N/mm^2 and 60 N/mm^2, respectively. Their interval change ratios are 0.2 and 0.15, respectively. The comparison between RLHNPSO and RQMCS for the mean value and standard deviation of interval random displacements at nodes B, C, D and E are shown in Table X. The convergence history of RLHNPSO for determining the intervals of the mean value of displacement at point C in X direction and at point E in X direction are illustrated in Figures 27 and 28, respectively. The deformed shape of the plate produced by the system parameters corresponding to the lower and upper mean value of displacement at point E in X direction and at point B in Y direction is respectively presented in Figures 29 and 30.

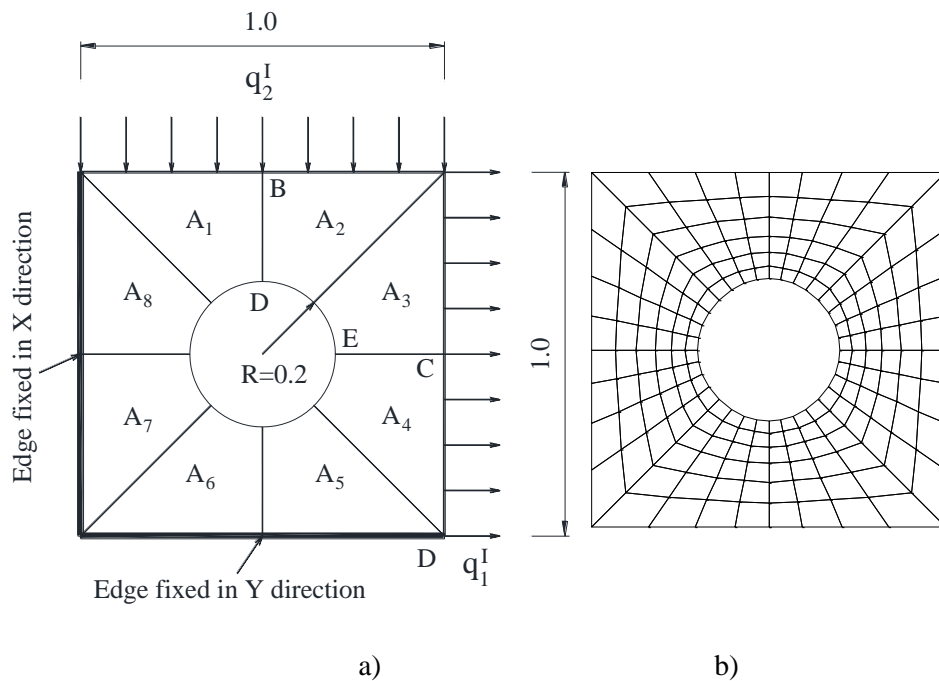a)   b)

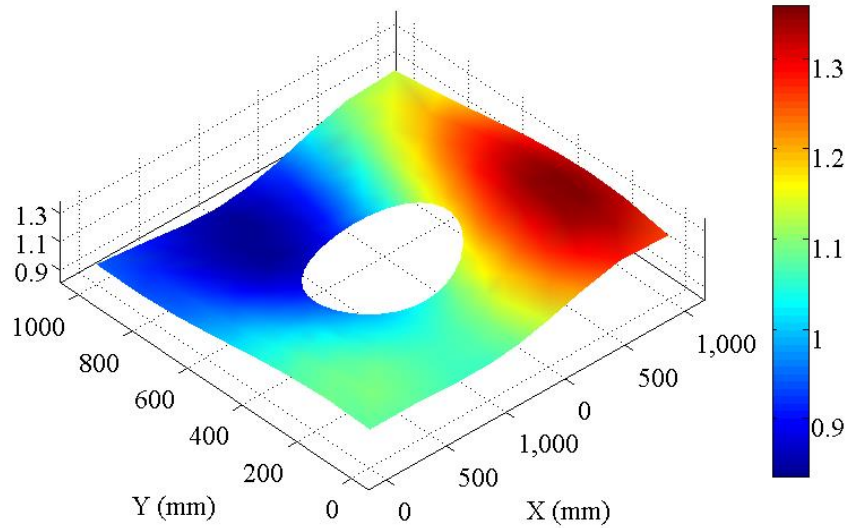Figure 25. 2D Plate with one hole: (a) geometry; (b) discretization.

Figure 26. A sample realization of the random field.

It can be observed that RLHNPSO has better performance with respect to faster convergence compared to RQMCS. This method can produce a wider range of target solutions than that of RQMCS, that is, the results obtained by RLHNPSO is more conservative. In other words, RLHNPSO can provide convergence results by less than $10 \times 40 = 400$ calculations, while other simulation methods cannot produce reliable results with a similar number of iterations. The time consuming for RLHNPSO to find the lower and upper bounds of mean value of displacement at node D in Y-direction is 3564.21 seconds while that for RQMCS is 42920.88 seconds which is approximately 12 times in comparison with the former. Again, it takes even longer if the number of iterations of RQMCS or MCS is increased to obtain better results. This test case was carried out on a computer equipped with a 3.30 GHz i5-2500 CPU.

Table X. Displacements derived from RLHNPSO and QMCS (unit: mm).

| Target solutions		Point B (Y-direction)		Point D (Y-direction)	
Methods		RQMCS	RLHNPSO	RQMCS	RLHNPSO
Mean	Upper	-0.60349	-0.59846	-0.53966	-0.53566
	Lower	-0.84317	-0.85148	-0.75290	-0.75927
Std	Upper	0.10290	0.10389	0.09257	0.09333
	Lower	0.07370	0.07309	0.06638	0.06590
Target solutions		Point C (X-direction)		Point E (X-direction)	
Methods		RQMCS	RLHNPSO	RQMCS	RLHNPSO
Mean	Upper	0.98329	0.98874	0.88318	0.88712
	Lower	0.67038	0.66596	0.60152	0.59792
Std	Upper	0.12045	0.12112	0.10838	0.10885
	Lower	0.08208	0.08155	0.07377	0.07334
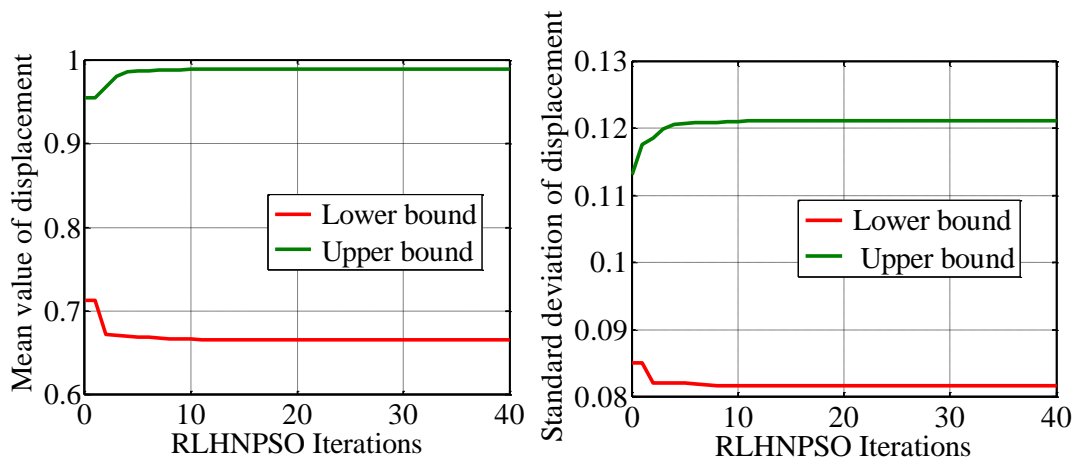
Figure 27. Convergence history of displacement at point C in X direction by RLHNPSO (unit: mm).
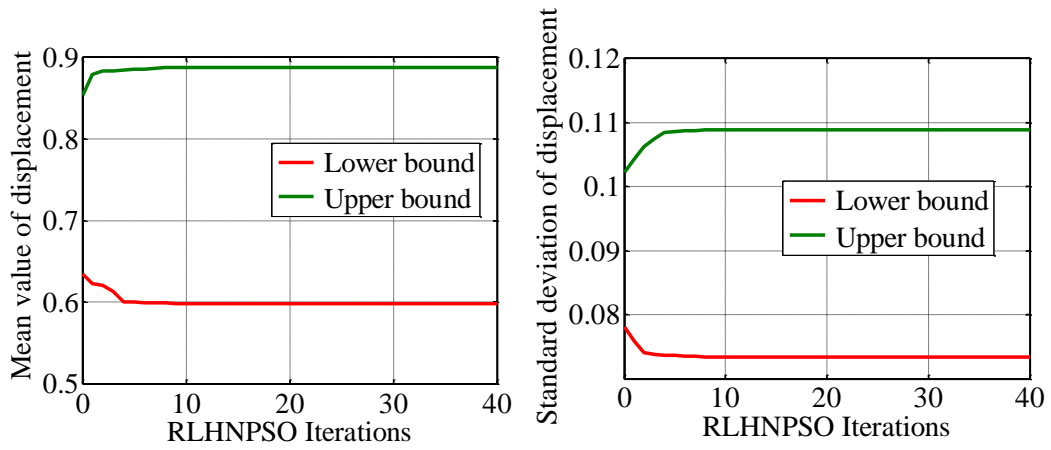

Figure 28. Convergence history of displacement at point E in X direction by RLHNPSO (unit: mm).
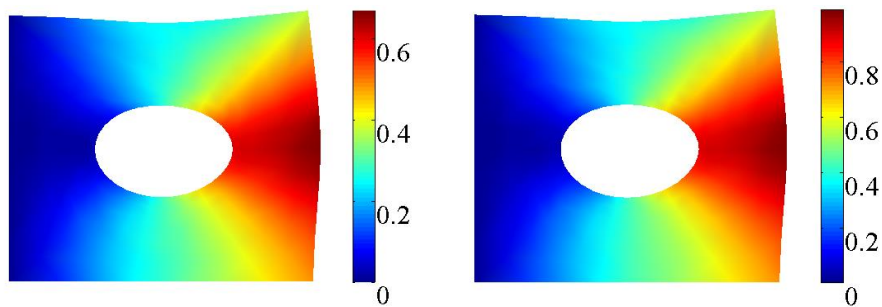

Figure 29. Deformed shape of mean of displacement at E in X-direction (unit: mm): (a) lower bound; (b) upper bound.
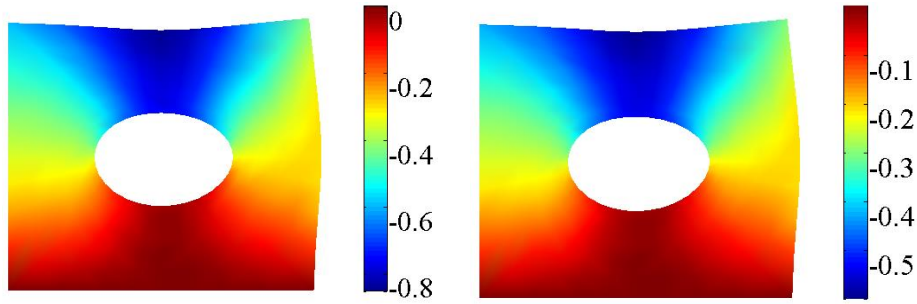
Figure 30. Deformed shape of mean of displacement at B in Y-direction (unit: mm): (a) lower bound; (b) upper bound.

The bounds of mean value of interval random displacement at point C in X direction are illustrated in Figure 31 by two response surfaces of undeformed shape S1 and S2. The former presents the responses of whole plate based on the input parameters are specified by the case of evaluating the lower bound for mean value of displacement at point C in X direction by means of RLHNPSO. The latter is the responses surface consistent with the attainment of the upper bound for mean value of displacement at point C in X direction by means of RLHNPSO. The mean value of the random interval displacement is not deterministic but interval as shown in Figure 31.
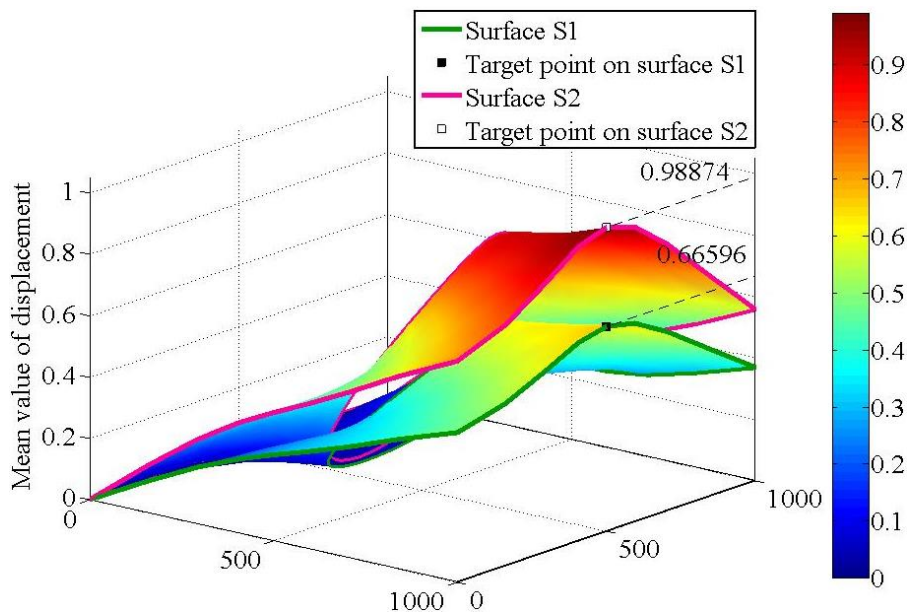

Figure 31. Bounded mean value of displacement at point C in X direction (unit: mm).

Another consideration in this test case is the parametric study on variability of results produced by RQMCS. The number of iterations for this method is varied to evaluate its performance. Results are given in Figures 32-35. Some detailed results are listed in Tables

VII and VIII. It appears that RQMCS is not capable of providing reliable results as with fluctuations of the responses produced by different number of iterations can be observed easily

Table XI. Statistical values of displacement at point D in Y direction derived by RQMCS with different number of iterations. Unit (mm).

Number of Iterations	Mean value		Standard deviation	
	Lower bound	Upper bound	Lower bound	Upper bound
2000	-0.75135	-0.54053	0.06649	0.09235
4000	-0.75380	-0.54106	0.06656	0.09266
6000	-0.75403	-0.54137	0.06659	0.09270
8000	-0.75210	-0.53981	0.06640	0.09246
10000	-0.75290	-0.53966	0.06638	0.09257
12000	-0.75424	-0.54170	0.06663	0.09272
14000	-0.75426	-0.54130	0.06659	0.09273
16000	-0.75442	-0.53983	0.06641	0.09275
18000	-0.75352	-0.53938	0.06634	0.09262
20000	-0.75425	-0.53916	0.06633	0.09273

Table XII. Statistical values of displacement at point C in X direction derived by RQMCS with different number of iterations. Unit (mm).

| Number of Iterations	Mean value		Standard deviation	
	Lower bound	Upper bound	Lower bound	Upper bound
2000	0.67438	0.97921	0.08256	0.11998
4000	0.67245	0.98058	0.08234	0.12010
6000	0.67130	0.98242	0.08219	0.12036
8000	0.67098	0.98066	0.08215	0.12016
10000	0.67038	0.98329	0.08208	0.12045
12000	0.67095	0.98444	0.08216	0.12060
14000	0.67073	0.98242	0.08212	0.12038
16000	0.67099	0.98128	0.08215	0.12021
18000	0.67069	0.98250	0.08213	0.12035
20000	0.67163	0.98138	0.08225	0.12024
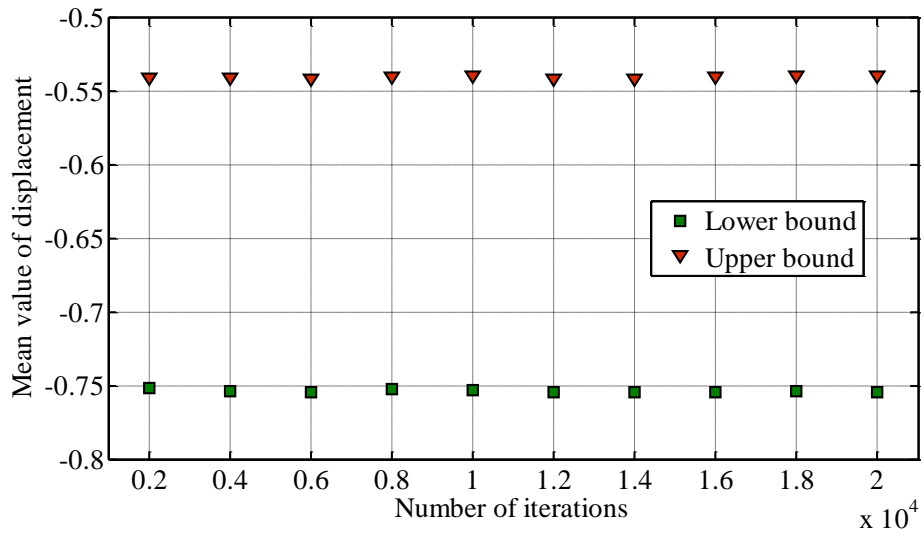
Figure 32. Mean value of displacement at point D in Y direction by RQMCS (unit: mm).
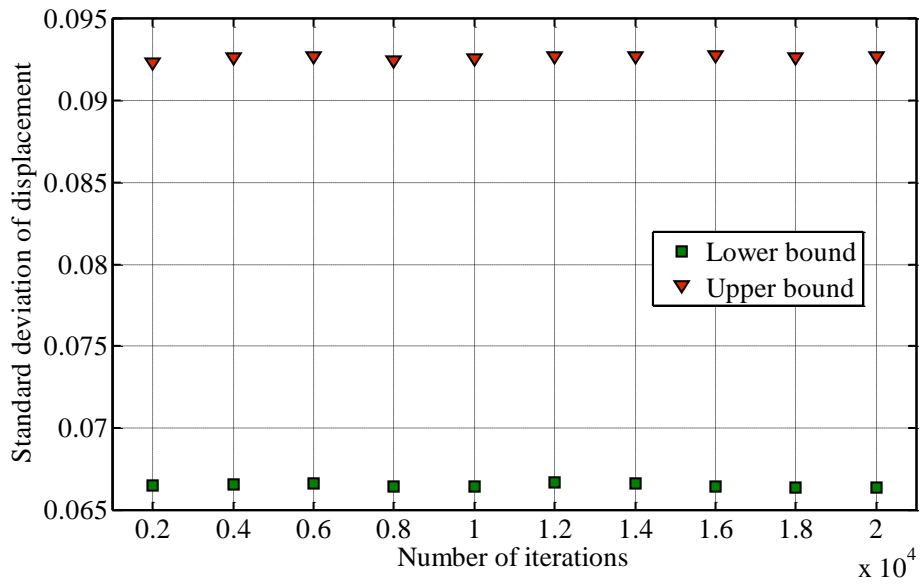

Figure 33. Standard deviation of displacement at point D in Y direction by RQMCS (unit: mm).
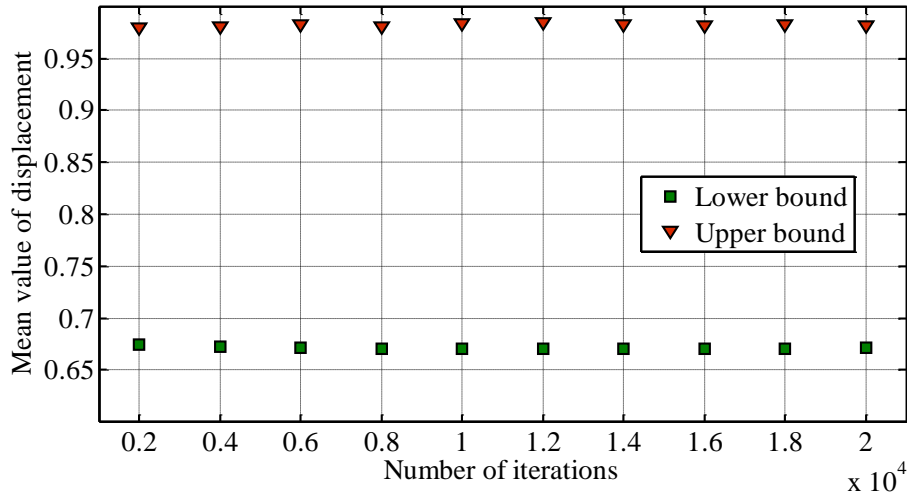
Figure 34. Mean value of displacement at point C in X direction by RQMCS (unit: mm).
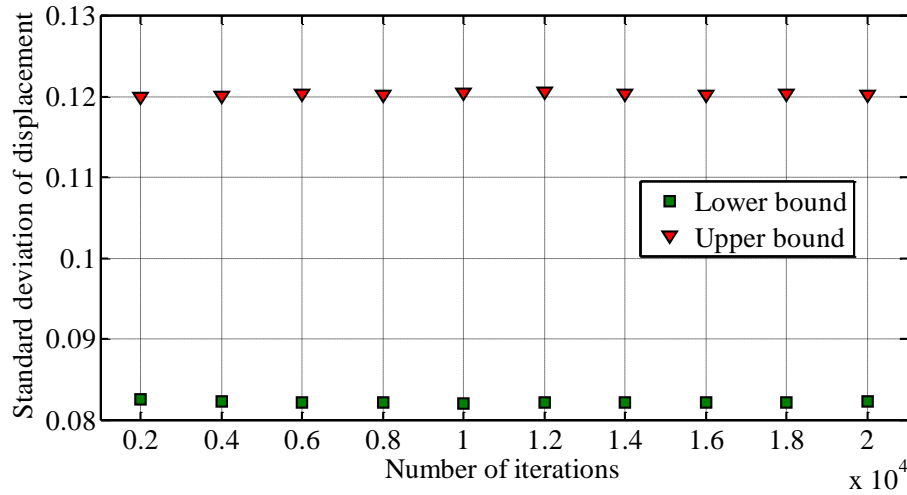

Figure 35. Standard deviation of displacement at point C in X direction by RQMCS (unit: mm).

5. CONCLUSION

Hybrid interval probabilistic analysis of structures with a combination of random fields and uncertain-but-bounded parameters is implemented in this study. The interval spectral stochastic finite element method (ISSFEM) is developed by incorporating the interval algorithm into the spectral stochastic finite element method (SSFEM). The proposed framework of ISSFEM has the ability to assess the effects of the random interval uncertainty of structures. Based on the K-L expansion and Polynomial Chaos, the random interval governing finite element equations are established, and the interval random structural responses are derived. Expressions for calculating the intervals for the mean value and the standard deviation of the interval random responses are obtained using the definition of statistical moments. An advanced evolutionary intelligence method, namely randomised low-

discrepancy sequences initialized high-order nonlinear particle swarm optimization algorithm (RLHNPSO), is adopted to determine the lower and upper bounds on the set of probabilistic models that characterize the interval random responses. The efficiency and accuracy of the proposed ISSFEM are validated through numerical examples. Compared with improved sampling in the form of randomized Quasi-Monte Carlo Simulation (RQMCS), which is used to handle interval uncertainty within the framework of ISSFEM, the RLHNPSO based hybrid interval stochastic method is capable of providing better solutions.

The presented methodology is applicable to pure random fields and interval problems as special cases. Hence, the proposed hybrid interval probabilistic analysis is an extension of established approaches and provides a technology for generalized uncertainty quantification and analysis. Further work is advisable to expand the applicability to very large structure and dynamic problems. This includes the further increase of numerical efficiency, but also an expansion to higher dimensionality to account for multi-random fields and high order multi-interval parameters. Also, extensions to accommodate non-linear behaviour would be meaningful.

ACKNOWLEDGEMENT

REFERENCES

1. Elishakoff I, Ren YJ, Shinozuka M. Some critical observations and attendant new results in the finite element method for stochastic problems. Chaos, Solitons & Fractals 1996;7:597-609.
2. Elishakoff I, Ren Y. The bird's eye view on finite element method for structures with large stochastic variations. Computer Methods in Applied Mechanics and Engineering 1999;168:51-61.
3. Schueller GI. Computational stochastic mechanics - recent advances. Computers & Structures 2001;79:2225-34.
4. Elishakoff I, Ren Y. Finite element methods for structures with large stochastic variations. Oxford ; New York: Oxford University Press; 2003.
5. Oden JT, Belytschko T, Babuska V, Hughes TJR. Research directions in computational mechanics. Computer Methods in Applied Mechanics and Engineering 2003;192:913-22.
6. Matthies HG, Brenner CE, Bucher CG, Soares CG. Uncertainties in probabilistic numerical analysis of structures and solids - Stochastic finite elements. Structural Safety 1997;19:283-336.
7. Ghanem RG, Spanos PD. Stochastic finite elements: a spectral approach: Springer-Verlag New York, Inc.; 1991.
8. Elishakoff I, Ren YJ, Shinozuka M. Conditional simulation of non-Gaussian random fields. Engineering Structures 1994;16:558-63.
9. Ghanem RG, Kruger RM. Numerical solution of spectral stochastic finite element systems. Computer Methods in Applied Mechanics and Engineering 1996;129:289-303.
10. Sudret B, Der Kiureghian A. Stochastic finite element methods and reliability: a state-of-the-art report. No. UCB/SEMM-2000/08 ed. University of California at Berkeley, USA 2000.
11. Anders M, Hori M. Three-dimensional stochastic finite element method for elasto-plastic bodies. International Journal for Numerical Methods in Engineering 2001;51:449-78.
12. Huang SP, Quek ST, Phoon KK. Convergence study of the truncated Karhunen–Loeve expansion for simulation of stochastic processes. International Journal for Numerical Methods in Engineering 2001;52:1029-43.

13. Chung DB, Gutierrez MA, Graham-Brady LL, Lingen FJ. Efficient numerical strategies for spectral stochastic finite element models. International Journal for Numerical Methods in Engineering 2005;64:1334-49.
14. Eiermann M, Ernst O, Ullmann E. Computational aspects of the stochastic finite element method. Computing and Visualization in Science 2007;10:3-15.
15. Stefanou G, Papadrakakis M. Assessment of spectral representation and Karhunen–Loève expansion methods for the simulation of Gaussian stochastic fields. Computer Methods in Applied Mechanics and Engineering 2007;196:2465-77.
16. Spanos PD, Beer M, Red-Horse J. Karhunen-loeve expansion of stochastic processes with a modified exponential covariance kernel. Journal of Engineering Mechanics-Asce 2007;133:773-9.
17. Ngah MF, Young A. Application of the spectral stochastic finite element method for performance prediction of composite structures. Composite Structures 2007;78:447-56.
18. Stefanou G. The stochastic finite element method: Past, present and future. Computer Methods in Applied Mechanics and Engineering 2009;198:1031-51.
19. Spanos PD, Zeldin BA. Monte Carlo Treatment of Random Fields: A Broad Perspective. Applied Mechanics Reviews 1998;51:219-37.
20. Spanos PD, Zeldin BA. Galerkin Sampling Method for Stochastic Mechanics Problems. Journal of Engineering Mechanics-Asce 1994;120:1091-106.
21. Ghanem R. Stochastic Finite Elements with Multiple Random Non-Gaussian Properties. Journal of Engineering Mechanics 1999;125:26-40.
22. Graham LL, Deodatis G. Response and eigenvalue analysis of stochastic finite element systems with multiple correlated material and geometric properties. Probabilistic Engineering Mechanics 2001;16:11-29.
23. Stefanou G, Papadrakakis M. Stochastic finite element analysis of shells with combined random material and geometric properties. Computer Methods in Applied Mechanics and Engineering 2004;193:139-60.
24. Chen N-Z, Guedes Soares C. Spectral stochastic finite element analysis for laminated composite plates. Computer Methods in Applied Mechanics and Engineering 2008;197:4830-9.
25. Moens D, Vandepitte D. A survey of non-probabilistic uncertainty treatment in finite element analysis. Computer Methods in Applied Mechanics and Engineering 2005;194:1527-55.
26. Beer M, Ferson S, Kreinovich V. Imprecise probabilities in engineering analyses. Mechanical Systems and Signal Processing 2013;37:4-29.
27. Schenk CA, Schueller GI. Uncertainty Assessment of Large Finite Element Systems. Lecture Notes in Applied and Computational Mechanics2005. p. 1-165.
28. Elishakoff I. Probabilistic methods in the theory of structures. New York: Wiley; 1983.
29. Beck JL. Bayesian system identification based on probability logic. Structural Control & Health Monitoring 2010;17:825-47.
30. Papadimitriou C, Beck JL, Katafygiotis LS. Updating robust reliability using structural test data. Probabilistic Engineering Mechanics 2001;16:103-13.
31. Jaynes ET, Bretthorst GL. Probability theory : the logic of science. Cambridge, UK ; New York, NY: Cambridge University Press; 2003.
32. Au SK. Connecting Bayesian and frequentist quantification of parameter uncertainty in system identification. Mechanical Systems and Signal Processing 2012;29:328-42.
33. Yan W-J, Katafygiotis LS. A novel Bayesian approach for structural model updating utilizing statistical modal information from multiple setups. Structural Safety.
34. Alvarez DA, Hurtado JE. An efficient method for the estimation of structural reliability intervals with random sets, dependence modeling and uncertain inputs. Computers & Structures 2014;142:54-63.
35. de Angelis M, Patelli E, Beer M. Advanced Line Sampling for efficient robust reliability analysis. Structural Safety 2015;52:170-82.
36. Beer M, Kreinovich V. Interval or moments: which carry more information? Soft Computing 2013;17:1319-27.
37. Moore RE. Interval Analysis: Prentice-Hall, Englewood Cliffs, N.J.; 1966.
38. Möller B, Beer M. Fuzzy Randomness: Uncertainty in Civil Engineering and Computational Mechanics: Springer; 2004.
39. Du XP, Sudjianto A, Huang BQ. Reliability-based design with the mixture of random and interval variables. Journal of Mechanical Design 2005;127:1068-76.
40. Gao W, Song C, Tin-Loi F. Probabilistic interval analysis for structures with uncertainty. Structural Safety 2010;32:191-9.
41. Jiang C, Li WX, Han X, Liu LX, Le PH. Structural reliability analysis based on random distributions with interval parameters. Computers & Structures 2011;89:2292-302.
42. Muscolino G, Sofi A. Stochastic analysis of structures with uncertain-but-bounded parameters via improved interval analysis. Probabilistic Engineering Mechanics 2012;28:152-63.

43. Jiang C, Long XY, Han X, Tao YR, Liu J. Probability-interval hybrid reliability analysis for cracked structures existing epistemic uncertainty. Engineering Fracture Mechanics 2013;112:148-64.

44. Beer M, Zhang Y, Quek ST, Phoon KK. Reliability analysis with scarce information: Comparing alternative approaches in a geotechnical engineering context. Structural Safety 2013;41:1-10.

45. Do DM, Gao W, Song C, Tangaramvong S. Dynamic analysis and reliability assessment of structures with uncertain-but-bounded parameters under stochastic process excitations. Reliability Engineering & System Safety 2014;132:46-59.

46. Wu JL, Luo Z, Zhang N, Zhang YQ. A new uncertain analysis method and its application in vehicle dynamics. Mechanical Systems and Signal Processing 2015;50-51:659-75.

47. Möller B, Beer M. Engineering computation under uncertainty – Capabilities of non-traditional models. Computers & Structures 2008;86:1024-41.

48. Moller B, Graf W, Beer M. Fuzzy structural analysis using alpha-level optimization. Computational Mechanics 2000;26:547-65.

49. Angelis Md, Patelli E, Beer M. Advanced Line Sampling for Efficient Robust Reliability Analysis. Structural Safety (accepted for publication).

50. Muhanna RL, Zhang H, Mullen RL. Interval finite elements as a basis for generalized models of uncertainty in engineering mechanics. Reliable Computing 2007;13:173-94.

51. Degrauwe D, Lombaert G, De Roeck G. Improving interval analysis in finite element calculations by means of affine arithmetic. Computers & Structures 2010;88:247-54.

52. Wu JL, Luo Z, Zhang YQ, Zhang N, Chen LP. Interval uncertain method for multibody mechanical systems using Chebyshev inclusion functions. International Journal for Numerical Methods in Engineering 2013;95:608-30.

53. Buras AJ, Jamin M, Lautenbacher ME. A 1996 analysis of the CP violating ratio epsilon'/epsilon. Physics Letters B 1996;389:749-56.

54. Rao SS, Berke L. Analysis of uncertain structural systems using interval analysis. AIAA Journal 1997;35:727-35.

55. Kennedy J, Eberhart R. Particle swarm optimization. Neural Networks, 1995 Proceedings, IEEE International Conference on1995. p. 1942-8 vol.4.

56. Xiaohui H, Eberhart RC, Yuhui S. Engineering optimization with particle swarm. Swarm Intelligence Symposium, 2003 SIS '03 Proceedings of the 2003 IEEE2003. p. 53-7.

57. Elbeltagi E, Hegazy T, Grierson D. Comparison among five evolutionary-based optimization algorithms. Advanced Engineering Informatics 2005;19:43-53.

58. Kreinovich V, Nguyen HT, Wu BL. On-line algorithms for computing mean and variance of interval data, and their use in intelligent systems. Information Sciences 2007;177:3228-38.

59. Ferson S, Ginzburg L, Kreinovich V, Longpr L, #233, Aviles M. Computing variance for interval data is NP-hard. SIGACT News 2002;33:108-18.

60. Oberkampf WL, Helton JC, Joslyn CA, Wojtkiewicz SF, Ferson S. Challenge problems: uncertainty in system response given uncertain parameters. Reliability Engineering & System Safety 2004;85:11-9.

61. Elishakoff I. Notes on philosophy of the Monte Carlo method. International Applied Mechanics 2003;39:753-62.

62. Oberkampf WL, DeLand SM, Rutherford BM, Diegert KV, Alvin KF. Error and uncertainty in modeling and simulation. Reliability Engineering & System Safety 2002;75:333-57.

63. Venter G, Sobieszczanski-Sobieski J. Multidisciplinary optimization of a transport aircraft wing using particle swarm optimization. Structural and Multidisciplinary Optimization 2004;26:121-31.

64. Perez RE, Behdinan K. Particle swarm approach for structural design optimization. Computers & Structures 2007;85:1579-88.

65. Plevris V, Papadrakakis M. A Hybrid Particle Swarm-Gradient Algorithm for Global Structural Optimization. Computer-Aided Civil and Infrastructure Engineering 2011;26:48-68.

66. Yildiz AR. A new hybrid particle swarm optimization approach for structural design optimization in the automotive industry. Proceedings of the Institution of Mechanical Engineers Part D-Journal of Automobile Engineering 2012;226:1340-51.

67. Parsopoulos KE, Vrahatis MN. Particle swarm optimizer in noisy and continuously changing environments. In: Hamza MH, editor. Artificial Intelligence and Soft Computing: IASTED/ACTA Press; 2001. p. 289-94.

68. Pant M, Thangaraj R, Grosan C, Abraham A. Improved Particle Swarm Optimization with Low-Discrepancy Sequences. IEEE World Congress on Computational Intelligence2008. p. 3011-8.

69. Liu NG, Gao W, Song CM, Zhang N, Pi YL. Interval dynamic response analysis of vehicle-bridge interaction system with uncertainty. Journal of Sound and Vibration 2013;332:3218-31.

70. Spanos PD, Ghanem R. Stochastic Finite-Element Expansion for Random-Media. Journal of Engineering Mechanics-Asce 1989;115:1035-53.